

Chemical evolution of Local Group dwarf galaxies in a cosmological context – I. A new modelling approach and its application to the Sculptor dwarf spheroidal galaxy

Donatella Romano^{1*} and Else Starkenburg^{2*†}

¹*INAF, Astronomical Observatory of Bologna, Via Ranzani 1, 40127 Bologna, Italy*

²*Department of Physics and Astronomy, University of Victoria, PO Box 3055 STN CSC, Victoria, BC, V8W 3P6, Canada*

Accepted 2013 June 7. Received 2013 June 7; in original form 2013 January 8

ABSTRACT

We present a new approach for chemical evolution modelling, specifically designed to investigate the chemical properties of dwarf galaxies in a full cosmological framework. In particular, we focus on the Sculptor dwarf spheroidal galaxy, for which a wealth of observational data exists, as a test bed for our model. We select four candidate Sculptor-like galaxies from the satellite galaxy catalogue generated by implementation of a version of the Munich semi-analytic model for galaxy formation on the level 2 Aquarius dark matter simulations and use the mass assembly and star formation histories predicted for these four systems as an input for the chemical evolution code. We follow explicitly the evolution of several chemical elements, both in the cold gas out of which the stars form and in the hot medium residing in the halo. We take into account in detail the lifetimes of stars of different initial masses, the distribution of the delay times for type Ia supernova explosions and the dependency of the stellar yields from the initial metallicity of the stars. We allow large fractions of metals to be deposited into the hot phase, either directly as stars die or through reheated gas flows powered by supernova explosions. We find that, in order to reproduce both the observed metallicity distribution function and the observed abundance ratios of long-lived stars of Sculptor, large fractions of the reheated metals must never re-enter regions of active star formation. With this prescription, all the four analogues to the Sculptor dwarf spheroidal galaxy extracted from the simulated satellites catalogue on the basis of luminosity and stellar population ages are found to reasonably match the detailed chemical properties of real Sculptor stars. However, all model galaxies do severely underestimate the fraction of very metal-poor stars observed in Sculptor. Our analysis thus sets further constraints on the semi-analytical models and, at large, on possible metal enrichment scenarios for the Sculptor dwarf spheroidal galaxy.

Key words: galaxies: abundances – galaxies: dwarf – galaxies: evolution – galaxies: formation – Local Group – cosmology: theory.

1 BACKGROUND AND MOTIVATION

Understanding how galaxies form and evolve is a major challenge to modern astrophysics. Crucial information on the sequence of events by which a stellar system took shape is encoded in the chemical composition of its stars. To fully exploit this information, large spectroscopic surveys of stars in the Milky Way and its neighbouring systems have been conceived, aimed at providing a complete picture of the chemical enrichment of the interstellar medium (ISM) back to the earliest epochs. At the same time, theoreticians have started to develop more sophisticated galaxy formation mod-

els (see, e.g., Font et al. 2011; Brook et al. 2012; Grieco et al. 2012; Pilkington et al. 2012; Revaz & Jablonka 2012, among others) to account for the unexpected features that are emerging from the data. In this context, studies of Local Group dwarf galaxies play a key role. The reason for this is, at least, threefold. Firstly, dwarf galaxies are the most common type of galaxy in the (local) Universe. As such, they bear the potential to study different star formation histories (SFHs) and their relation with the environment in a large, statistically significant sample of objects of the same class. Secondly, our capability to resolve Local Group dwarfs’ stellar populations makes them ideal test beds for theories of galaxy formation and evolution on small scales (see next paragraphs). Thirdly, small systems are the fundamental building blocks for the assembly of larger galaxies in Cold Dark Matter (CDM) cosmological models (White & Rees 1978; White & Frenk 1991). It has been well es-

* E-mail: donatella.romano@oabo.inaf.it (DR); else@uvic.ca (ES)

† CIFAR Junior Fellow and CITA National Fellow.

established on the basis of chemical arguments (e.g. Shetrone et al. 2001) that the Galactic halo could not form through merging of low-mass galaxies resembling the dwarf spheroidals orbiting the Milky Way *today*. However, very and extremely metal-poor stars belonging to different environments display more similar chemical abundance patterns (of, in particular, α and heavy elements; e.g. Tolstoy et al. 2009). This has renewed the interest in the connection between *ancient* dwarf galaxies and the primeval building blocks of the Galactic halo.

Both classical bright and faint Local Group dwarf galaxies are close enough to allow their chemical enrichment and star formation histories to be derived with great precision from high-quality measurements of individual stars (Tolstoy et al. 2009, and references therein), which provides tight constraints on simulations of the chemical and dynamical evolution of such systems. In particular, the adoption of the ‘true’ SFH and stellar initial mass function (IMF) derived from analyses of the colour-magnitude diagrams (CMDs) allows us to remove some important parameters of chemical evolution and leads to a more sound modelling of specific objects (Carigi et al. 2002; Lanfranchi & Matteucci 2003, 2004; Romano et al. 2006).

Dwarf galaxies should be prone to considerable loss of matter through galactic winds originating from multiple SN explosions, because of their shallow potential wells. Galactic winds have been discussed in theory (Larson 1974; Saito 1979; Matteucci & Chiosi 1983; Matteucci & Tosi 1985; Dekel & Silk 1986; Vader 1987; Pilyugin 1993, among others) long before the observational evidence for them in dwarfs became clear-cut (Meurer et al. 1992; Martin 1999; Heckman et al. 2001; Martin et al. 2002; see also Veilleux et al. 2005, and references therein). Nowadays, galactic-scale outflows are often invoked as the most suited explanation for the low mass densities, metallicities and detailed chemical abundance ratios of star-forming dwarfs (e.g. Yin et al. 2011). Yet, a sound theory of galactic winds is missing. In particular, it is still debated whether the SN ejecta can leave the galaxy definitively or cool down and be reaccreted; moreover, it is still unclear which fraction of the ambient gas is entrained in the outflow and how metals are loaded (Silich & Tenorio-Tagle 1998; D’Ercole & Brighenti 1999; Mac Low & Ferrara 1999; Ferrara & Tolstoy 2000; Tenorio-Tagle et al. 2007; Recchi & Hensler 2013; see also Heckman et al. 2001; Summers et al. 2001, 2003; Martin et al. 2002; Cannon et al. 2004; Oppenheimer & Davé 2006; Peebles & Shankar 2011).

When modelling the chemical evolution of dwarf galaxies with estimated SFHs, the final fate and chemical composition of the outflow are only one of the major sources of uncertainty. We still do not know when or how the gas is accreted, or how efficiently it is turned into stars. Recent or ongoing star formation activity in several dwarf irregular galaxies (dIrrs) and blue compact dwarfs (BCDs) is clearly associated to accretion of neutral gas, either through infall or gas-rich body encounters (e.g. Putman et al. 1998; Stil & Israel 2002; Pustilnik et al. 2003; Kobulnicky & Skillman 2008). Starbursting dwarfs with no obvious external trigger mechanism could still have faint undetected companions (see Hunter & Elmegreen 2004, and references therein). On the other hand, the presence of neutral gas does not assure ongoing star formation by itself. Photoionization, heating from the cosmic ultraviolet (UV) background, tidal interactions and ram pressure stripping are further processes that may leave an imprint on the observed properties of dwarf galaxies and should be accounted for in the models.

In dealing with the above issues, classical chemical evolution models for dwarf galaxies tend to keep things simple. They do not

take into account reionization, tidal interactions or stripping of gas and/or stars, and introduce a number of free parameters and simplifying assumptions about the dark matter mass and distribution, the stellar feedback efficiency and the history of mass assembly. In particular, a time-decaying gas infall rate is usually assumed (e.g. Chiosi & Matteucci 1982; Matteucci & Chiosi 1983; Bradamante et al. 1998; Mouhcine & Contini 2002; Yin et al. 2011), following dynamical studies of the collapse of protogalaxies dating to Larson (1976). An infall rate increasing with time, simulating the late accretion of gaseous lumps, was adopted by Romano et al. (2006) for the specific case of NGC 1569, an exceptionally active nearby dIrr, and shown to nicely reproduce the observed properties of that galaxy. However, no physical explanation was given for the assumed infall law. Models without inflow have also been proposed in the literature (e.g. Carigi et al. 1995).

Cosmological simulations provide crucial information on the mass assembly history of galaxies and, hence, a tempting framework for chemical evolution studies, since they remove the need for some *ad hoc* prescriptions. In turn, the chemical evolution models have the capability to screen many different realizations for a given object—or class of objects—and look for the evolutionary path that maximizes the agreement between the observed and predicted detailed chemical properties. Chemical evolution studies thus offer a way to further constrain the parameters entering *ab initio* galaxy formation models. So far, a number of studies has been devoted to the chemical evolution of galaxies within a hierarchical clustering scheme (Thomas 1999; Nagashima et al. 2005; Nagashima & Okamoto 2006; Pipino et al. 2009; Arrigoni et al. 2010; Rahimi et al. 2011; Brook et al. 2012), with some attempts to deal with local dwarfs (Salvadori et al. 2008; Calura & Menci 2009; Okamoto et al. 2010; Sawala et al. 2010; Pilkington et al. 2012; Revaz & Jablonka 2012). Most of these works, however, consider only a few chemical species; moreover, the contribution of the low- and intermediate-mass stars (LIMS) is often neglected: this prevents a proper treatment of elements such as He, C and N, that are precious diagnostics of chemical evolution, especially in dIrrs and BCDs (e.g. James et al. 2010), as well as important gas coolants (Wiersma et al. 2009). In some cases, type Ia SNe (SNeIa)—the major iron producers—are not included in the models.

In this work, we present a new chemical evolution model, specifically designed to follow the evolution of the abundances of several elements (H, D, He, Li, C, N, O, Na, Mg, Al, Si, S, Ca, Sc, Ti, Cr, Mn, Co, Ni, Fe, Cu, Zn) in the hot and cold gas phases of dwarf galaxies in a cosmological context. The lifetimes of stars of different initial masses and the distribution of the delay times for SNIa explosions are taken into account in detail, as is the dependency of the yields on the initial metallicity of the stars. We choose the Sculptor dwarf spheroidal galaxy (dSph) as a test bed for our model, because of the conspicuous body of high-quality observational data available in this case to calibrate the model parameters. First, four Milky Way satellites resembling Sculptor in luminosity and SFH are identified in the satellite catalogue generated by Starkenburg et al. (2013a) through the implementation of a version of the Munich semi-analytic model (SAM) for structure formation (De Lucia & Blaizot 2007; De Lucia et al. 2008; Li et al. 2009, 2010) on the high resolution level 2 Aquarius dark matter simulations (Springel et al. 2008a,b). Then, the detailed chemical properties of the four Sculptor candidates are computed from the full cosmological mass assembly histories and including the response to a variety of internal and external physical processes, such as photoionization, heating from the cosmic UV background, star

formation, SN feedback, tidal interactions and ram pressure stripping.

This paper is organized as follows. Section 2 summarizes seven decades of investigation of the Sculptor dSph, highlighting the latest results. Section 3 contains a brief description of the adopted cosmological simulations and semi-analytical model, along with a detailed description of the post-processing chemical evolution code that we have developed. Section 4 follows with a presentation of the results concerning the detailed chemical properties of our four Sculptor candidates. We furthermore point out the dependence of the results on model parameters in Section 4. The strengths and shortcomings of our approach are discussed in Section 5, also in comparison with previous work. We conclude with a summary and prospects for future work in Section 6.

2 THE SCULPTOR DWARF SPHEROIDAL GALAXY

Since its discovery late in the thirties (Shapley 1938), the Sculptor dwarf spheroidal galaxy (dSph) has been the subject of extensive investigation. Sculptor is a relatively faint ($M_V \approx -11.1$; Irwin & Hatzidimitriou 1995; Mateo 1998) stellar system, located 86 ± 5 kpc away from us (Pietrzyński et al. 2008). The bulk of its stars are old (>10 Gyr old; Da Costa 1984), with a small tail of stars at intermediate ages (6–10 Gyr; Dolphin 2002; Tolstoy et al. 2003). A metallicity gradient is present in Sculptor (Tolstoy et al. 2004), which is linked to an age gradient (de Boer et al. 2011). Younger and more metal-rich stars concentrate towards the centre. Under the hypothesis that Sculptor is not tidally disrupted, Battaglia et al. (2008a) have estimated its total mass to be $\mathcal{M}_{\text{tot}}(<1.8 \text{ kpc}) = (3.4 \pm 0.7) \times 10^8 M_\odot$, making it more massive than previously thought.

Recently, a very accurate SFH of Sculptor has been derived from deep, wide-field CMDs covering a large fraction of the galaxy and going down to the oldest main sequence turn-off (de Boer et al. 2011, 2012). The basic features found in previous works have been confirmed: star formation took place in Sculptor at early epochs and lasted several Gyr, from 14 to 7 Gyr ago. During this period, the star formation proceeded at a steadily decreasing rate (see de Boer et al. 2012, their figure 8).

The first studies of detailed chemical abundances in Sculptor are those of Shetrone et al. (2003) and Geisler et al. (2005). They used the Ultraviolet Echelle Spectrograph (UVES) on the Very Large Telescope (VLT) to determine the abundances of several elements in 5 and 4 red giant branch (RGB) stars, respectively. Notwithstanding the low number of stars probed, it was immediately clear that the Sculptor dSph follows a chemical enrichment path distinct from that of any of the Milky Way components. In the last few years, thanks to the high multiplex capabilities of instruments such as DEIMOS (Deep Imaging Multi-Object Spectrometer) on Keck II and FLAMES (Fibre Large Array Multi Element Spectrograph) on VLT, detailed abundances of several elements have become available for hundreds of stars in Sculptor (Kirby et al. 2009, 2010; North et al. 2012; Hill et al., in preparation, see Tolstoy et al. 2009). Tight $[X/\text{Fe}]$ – $[\text{Fe}/\text{H}]$ relations have been found in the metallicity range $-2.5 \leq [\text{Fe}/\text{H}] \leq -1.0$; in particular, the $[\alpha/\text{Fe}]$ ratio has been found to steadily decline with metallicity. For a handful of extremely metal-poor stars below $[\text{Fe}/\text{H}] \sim -3.5$ dex, a detailed analysis of the abundances of the α , iron-peak and heavy elements has been carried out using high-resolution spectra taken with Magellan/MIKE (Frebel et al. 2010) and VLT/UVES (Tafelmeyer et al. 2010). Most recently, Starkenburg et al. (2013b) have enlarged

the sample of (extremely) low metallicity stars by adding seven objects with detailed chemical abundances from spectra taken with X-shooter on the VLT.

A well-defined stellar metallicity distribution function (MDF) for Sculptor has been obtained from wide-field medium resolution Ca II triplet spectroscopy of more than 600 RGB stars (Battaglia et al. 2008b; Starkenburg et al. 2010). Kirby et al. (2010) also present the MDF of Sculptor’s stars, for a smaller sample of <400 objects. The shape of the MDFs from both studies is expected to be different due to the different depth and radial extent of their data sets. There is good agreement for the $[\text{Fe}/\text{H}]$ values for stars in common between both datasets and the high-resolution study of Hill et al. (in preparation). The MDF we use for comparison with our model results in Sect. 4 combines both data sets in an attempt to mitigate the biases affecting individual studies (see Appendix A for details about the derivation of our more unbiased MDF).

The trend of the abundance ratios with $[\text{Fe}/\text{H}]$ and the shape of the MDF supply complementary information on the timescales of chemical enrichment in Sculptor and provide an unprecedented benchmark for chemical evolution studies. We will take advantage of the wealth of available data to sensibly constrain the free parameters of our model.

3 THE MODEL

Starkenburg et al. (2013a) have studied the satellites of the Milky Way by using a SAM of galaxy formation coupled to high-resolution N -body cosmological simulations. Their model galaxies match several observed relations on the scale of the Milky Way and its satellites. The dwarf galaxies display large variations in their SFHs, as observed. Based on the SFHs, model satellites are identified that crudely resemble the Carina, Sculptor and Fornax dSphs. The predicted MDFs, however, are too narrow with respect to the observed ones (see Starkenburg et al. 2013a, their figure 13). As discussed by the authors, this discrepancy is likely largely due to the adoption of the instantaneous recycling approximation (IRA) in their study and certainly deserves further analysis.

In this paper, we compute the detailed chemical enrichment history of four Sculptor-like dwarf galaxies identified from Starkenburg et al. (2013a; see their figures 12 and 13 for SFHs and metallicity distributions of models labelled Scl 1–3 here, the fourth model labelled Scl 4 was additionally selected for this work). The Sculptor-like galaxies are selected on coarse luminosity ($-11.8 < M_V < -10.3$) and dominant old stellar population criteria. In Sections 3.1 and 3.2 we concisely describe the adopted cosmological framework and semi-analytic modelling. In Section 3.3 we present the post-processing code that we have developed to compute the evolution of chemical abundances in hierarchically growing systems. In forthcoming papers of this series (Romano et al., in preparation; Starkenburg et al., in preparation), we enlarge our sample and test the predictions for satellite versus isolated objects.

3.1 The cosmological simulations

For the Aquarius project (Springel et al. 2008a) six halos were selected from the lower resolution fully cosmological parent simulation, Millennium II, and resimulated at much higher resolution. The results in this work were obtained from the level 2 Aquarius simulations with a particle mass around $\sim 1 \times 10^4 M_\odot$. Tests on different resolution runs, spanning a maximum range in particle mass of a factor of 1800 in halo A, show remarkably good convergence

exceeding any previous efforts (Springel et al. 2008a). Although the cosmological parameters used for the simulation were based on the first-year results from the Wilkinson Microwave Anisotropy Probe (WMAP) satellite and are no longer consistent with the latest WMAP analysis (Komatsu et al. 2011), we do not expect this to affect the results presented here significantly. Wang et al. (2008), for instance, demonstrate that it is difficult to distinguish between WMAP1 and WMAP3 in combination with SAMs for low-redshift galaxies. Guo et al. (2013) make a similar comparison between WMAP1 and WMAP7. They use the Millennium-II simulation, which allows for the formation of galaxies down to $\sim 10^8 M_\odot$, i.e. closer to the predicted mass of Sculptor.

The six main halos were selected to have dark matter masses in the range of $0.8\text{--}1.8 \times 10^{12} M_\odot$, consistent with the estimated mass for the Milky Way (e.g. Wilkinson & Evans 1999; Sakamoto et al. 2003; Battaglia et al. 2005; Smith et al. 2007; Li & White 2008; Xue et al. 2008; Guo et al. 2010). The dark matter substructures that are the main interest for our work, are identified using the code SUBFIND (Springel et al. 2001), which identifies self-bound structures within each friends-of-friends group. A lower mass limit of 20 particles is used in identifying the substructures. We refer the reader to Springel et al. (2008a,b) for further information concerning the Aquarius simulations and to Springel et al. (2001) for a description of SUBFIND.

3.2 The semi-analytical model

Substructure catalogues are used to construct merger history trees for all self-bound halos and subhalos in the Aquarius simulations (Springel et al. 2005; De Lucia & Blaizot 2007), which we are using as a backbone for further modeling. In this semi-analytical approach we follow relevant physical processes to study the flows and fate of baryons using relatively simple expressions which are motivated and supported by observations wherever possible. Our specific model applied for this work was described in Starkenburg et al. (2013a) and stems from the models described in Kauffmann et al. (1999), Springel et al. (2001) and De Lucia et al. (2004). Subsequent updates have been made by Croton et al. (2006) and De Lucia & Blaizot (2007) and several minor adaptations were made to the model by De Lucia et al. (2008), Li et al. (2009, 2010) and Starkenburg et al. (2013a) to model more adequately the physics of galaxy formation and evolution within the scale of a Milky Way environment.

Physical processes modeled include reionization, cooling, star formation, SN feedback and tidal stripping. A schematic diagram of several main processes modeled and their interaction, is shown in Fig. 1. We refer the interested reader to Starkenburg et al. (2013a, and references therein) for a detailed description of the semi-analytical prescriptions. However, in order to enable a comparison with the numerical model for chemical evolution used for the post-processing in this work (see Section 3.3), a review of the star formation and feedback prescriptions is given below.

The SFH is governed within the model by the amount of cold gas above a critical density threshold within each system at each time,

$$\psi = \varepsilon \mathcal{M}_{\text{sf}} / t_{\text{dyn}}, \quad (1)$$

where $\varepsilon = 0.03$ represents the efficiency of the conversion of gas into stars, \mathcal{M}_{sf} is the cold gas mass eligible for star formation (which is assumed to form an exponential disk; see Mo et al. 1998 for prescriptions) and $t_{\text{dyn}} = r_{\text{disk}} / V_{\text{vir}}$ is the dynamical time of

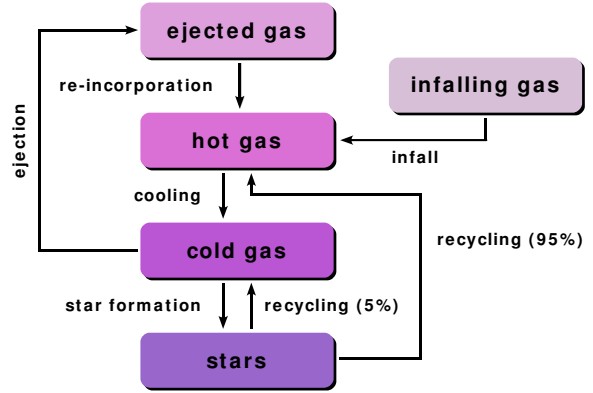


Figure 1. A schematic chart of the flows of baryons in the adopted SAM. The boxes represent the different phases of the baryons. The arrows show how the baryons change phase, owing to the different processes that affect them. Notice that in the ‘*ejection model*’ adopted in this paper 95 per cent of newly produced metals are actually deposited directly in the hot phase. Not shown here are the processes of stripping. They can affect all phases and are implemented in the model though.

the disk. Following Kennicutt (1989), the critical density threshold for star formation is

$$\frac{\Sigma_{\text{crit}}}{M_\odot \text{pc}^{-2}} = 0.59 \frac{V_{\text{vir}}}{\text{km s}^{-1}} / \frac{r_{\text{disk}}}{\text{kpc}}. \quad (2)$$

A second, bursty mode of star formation is possible during minor or major mergers, when (part of) the cold gas in the merging galaxies is turned into stars. The model assumes that photo-dissociation from UV radiation will prevent cooling from molecular hydrogen, thus does not allow gas to cool in halos whose virial mass corresponds to a temperature below 10^4 K (the atomic hydrogen cooling limit). This implies that the model does not take into account a physical implementation of the first stars, which most likely have to be cooled through the molecular hydrogen channel. A proper implementation of first star physics would require assumptions on the interplay between molecular hydrogen cooling and dissociation, as well as the IMF for the first stars, which are not well understood.

Within the SAM, IRA is adopted, meaning that immediate SN feedback is modeled from the stars and that their finite ages are not taken into account by the model. The recycled fraction, defined to be the ratio of the amount of recycled gas to the total amount of gas that was initially converted into stars, is 43 per cent in the SAM, using a Chabrier IMF. The feedback recipe used is identical to the ‘*ejection model*’ described in Li et al. (2009, 2010), where 95 per cent of the SN ejecta goes directly in the hot phase, and includes a dependence on the halo potential well (i.e. $\propto 1/V_{\text{vir}}^2$) to determine the amount of cold gas affected by the energy output from SNe. The fraction of SN ejecta that is instantaneously returned to the ISM (5 per cent) is mixed with the cold gas before reheating. The reheated cold material is stored in a separated component of ejected gas and can be reincorporated into the hot gas reservoir available at later times. In the majority of this work, we assume reheated cold gas never returns to the ISM. However, we also test the effect of allowing some of it to return at later times (see Sect. 4.3.3).

3.3 The galactic chemical evolution tool

The information as schematically represented in Fig. 1 is subsequently post-processed to determine the chemical evolution of the galaxy. We use the full history for the galaxy, including possible merging events. For each baryonic state described in Fig. 1, the information from all progenitors is added together. We note, however, that late (major) merging events are rare in all our Sculptor-type galaxies that typically become a satellite of the Milky Way-like galaxy quite early in their life. The adopted SAM additionally does not provide spatially resolved information about the baryonic content within the targeted galaxies. Therefore, we use a one zone approximation and follow the evolution of tracked elements in the cold gas out of which stars form irrespective of which progenitor they formed in or the distance from the galaxy centre, by means of the following equations:

$$\frac{d\mathcal{M}_i(t)}{dt} = -X_i(t)\psi(t) + (1-F)\mathcal{R}_i(t) + \frac{d\mathcal{M}_i^{\text{in}}(t)}{dt} - \frac{d\mathcal{M}_i^{\text{out}}(t)}{dt}, \quad (3)$$

where $\mathcal{M}_i(t) = X_i(t)\mathcal{M}_{\text{cold}}(t)$ is the cold gas mass in the form of the element i at the time t , $X_i(t)$ is the abundance by mass of the element i in the cold gas at the time t and the summation of all $X_i(t)$ is equal to unity. $\psi(t)$ is the star formation rate (SFR), $\mathcal{R}_i(t)$ is the production rate of the element i by dying stars. F is the fraction of the stellar ejecta that goes directly into the hot gas phase (see previous section and Li et al. 2010). The last two terms on the right-hand side of equation (3) account for the addition/loss of element i to/from the cold gas phase owing to: (i) cooling of hot gas, (ii) interactions with other galaxies[‡] and (iii) ejection of gas heated by SN explosions. The main physical processes entering the right-hand side of equation (3) are sketched in Fig. 1.

3.3.1 Stellar nucleosynthesis

In our model, the production rate of the element i at the time t is computed by taking into account in detail the contributions of stars of different initial masses (lifetimes) and chemical compositions (using the Q -matrix formalism; Talbot & Arnett 1973), as well as the presence of binary systems ending up as SNeIa:

$$\mathcal{R}_i(t) = \mathcal{R}_i^{\text{LIMS}}(t) + \mathcal{R}_i^{\text{SNII}}(t) + \mathcal{R}_i^{\text{SNIa}}(t). \quad (4)$$

$\mathcal{R}_i^{\text{LIMS}}(t)$, $\mathcal{R}_i^{\text{SNII}}(t)$ and $\mathcal{R}_i^{\text{SNIa}}(t)$ are the rates at which low- and intermediate-mass stars, core-collapse SNe and SNeIa, respectively, restore each element to the ISM. For low- and intermediate-mass stars, it reads

$$\mathcal{R}_i^{\text{LIMS}}(t) = (1-\mathcal{B}) \int_{m_l(t)}^{m_{\text{WD}}} \varphi(m)\psi(t-\tau_m)\mathcal{Q}_{mi}(t-\tau_m)dm, \quad (5)$$

where $m_l(t)$ is the turn-off mass at the time t , $m_{\text{WD}} = 8 M_{\odot}$ is the maximum mass for white dwarf formation, τ_m is the lifetime of the star of initial mass m , $\varphi(m)$ is the IMF. Here we interpolate linearly between tabulated stellar lifetimes from Schaller et al. (1992) and assume an extrapolation of the Salpeter (1955) IMF in the mass range 0.1–100 M_{\odot} , unless otherwise stated. Following Maeder (1992), the quantities $\mathcal{Q}_{mi}(t-\tau_m)$ are the summation of two terms,

$$\mathcal{Q}_{mi}(t-\tau_m) = X_i(t-\tau_m)m_{\text{ej}}(m) + mp_i(m), \quad (6)$$

[‡] Both our SAM and chemical post-processing code have in principle the ability to deal with tidal stripping of gas, as well as stars. In the specific models studied such events do not occur however.

that consistently compute the mass ejected in the form of the element i that was already present at the stellar birth—first term on the right-hand side of equation (6)—and the newly synthesized one according to specific yields tables—second term on the right-hand side of equation (6); $m_{\text{ej}}(m)$ and $p_i(m)$ are, respectively, the total mass ejected by a star of mass m during its lifetime and the stellar yield (Tinsley 1980). The quantity \mathcal{B} is the realization probability for SNeIa. It is a free parameter of the model and is different from zero only in a restricted mass range (3–16 M_{\odot} ; see next paragraph). Here $\mathcal{B} = 0.03$, i.e. we set \mathcal{B} to the same value which allows us to reproduce the present-day SNIa rate in the disk of the Milky Way (Li et al. 2011). Similarly, for massive stars,

$$\mathcal{R}_i^{\text{SNII}}(t) = (1-\mathcal{B}) \int_{m_{\text{cc}}}^{m_u} \varphi(m)\psi(t-\tau_m)\mathcal{Q}_{mi}(t-\tau_m)dm, \quad (7)$$

where $m_u = 100 M_{\odot}$ is the upper mass limit of the IMF and $m_{\text{cc}} = 8 M_{\odot}$ is the minimum mass for core-collapse SNe.

The rate at which SNeIa restore their nucleosynthetic products to the ISM is a strong function of the adopted SFR and progenitor model and, to a lesser extent, of the adopted stellar lifetimes and IMF (Greggio & Renzini 1983; Matteucci & Greggio 1986; Kobayashi et al. 1998; Matteucci & Recchi 2001; Greggio 2005; Matteucci et al. 2006, 2009; Kobayashi & Nomoto 2009). Following Greggio & Renzini (1983) and Matteucci & Greggio (1986), it can be written

$$\mathcal{R}_i^{\text{SNIa}}(t) = \mathcal{B} \int_{m_{\text{b,min}}(t)}^{m_{\text{b,max}}(t)} \varphi(m_{\text{b}}) \int_{\mu_{\text{min}}}^{\mu_{\text{max}}} f(\mu) \psi(t-\tau_{m_2})\mathcal{Q}_{m_1 i}(t-\tau_{m_2})d\mu dm_{\text{b}}, \quad (8)$$

where $m_{\text{b}} = m_1 + m_2$ is the total mass of the binary system and $\mu = m_2/m_{\text{b}}$. The masses $m_{\text{b,min}}(t)$ and $m_{\text{b,max}}(t)$ are the minimum and maximum masses, respectively, of the contributing systems at the time t ; the minimum and maximum values that they can take are 3 M_{\odot} and 16 M_{\odot} , respectively. $f(\mu)$ is the distribution function for the mass of the secondary star with respect to the total mass of the system and is taken from Greggio & Renzini (1983), with $\mu_{\text{min}} = \max(m_2/m_{\text{b}}, (m_{\text{b}} - 8)/m_{\text{b}})$, $\mu_{\text{max}} = 0.5$. The lifetime of the secondary star, τ_{m_2} , is the clock for the explosion. We refer to Matteucci & Recchi (2001, and references therein) for more details. We remark that no metallicity effect leading to the inhibition of SNeIa at low metallicity (Kobayashi et al. 1998; Kobayashi & Nomoto 2009) is included in the present work. We will analyze the effect of adopting different prescriptions for SNeIa on our model results in a forthcoming paper.

As for single stars, in this work we adopt the metallicity-dependent yields from van den Hoek & Groenewegen (1997) for LIMS and Woosley & Weaver (1995) for massive stars. Uncertainties in the iron yields are a factor of two; following Timmes et al. (1995), we halve the yields of iron from massive stars in the original Woosley & Weaver’s tables (see also Goswami & Prantzos 2000; Romano et al. 2010a). As for binary systems giving rise to SNIa events, we use Iwamoto et al.’s (1999) yields (their model W7) apart from Mn, for which we use the prescriptions of Cescutti et al. (2008; see also Romano et al. 2011). It is worth emphasizing that this combination of stellar yields ensures a good fit to the $[X/\text{Fe}]$ – $[\text{Fe}/\text{H}]$ relations of most chemicals in the solar neighbourhood, at metallicities typical of dSphs (Romano et al. 2010a, their figure 22, model 1). In general, our code is structured in such a way that it can be easily supplied with different yield sets.

3.3.2 Gas flows and star formation: the cosmological context

In the classical approach (see next section), the dwarf galaxy is treated as an isolated object, with a smooth accretion of infalling gas. For the models computed in a cosmological context, we adopt the SFH and gas flows from the cosmological simulations and SAM described in Sects. 3.1 and 3.2. It reads:

$$\frac{d\mathcal{M}_i^{\text{in}}(t)}{dt} = X_i^{\text{cool}}(t) \frac{d\mathcal{M}_{\text{cool}}(t)}{dt}, \quad (9)$$

where $X_i^{\text{cool}}(t) = X_i^{\text{hot}}(t)$ is the abundance by mass of the element i in the cooling flow at the time t and $\mathcal{M}_{\text{cool}}(t)$ is the total mass accreted from the hot gas reservoir at the time t , and

$$\frac{d\mathcal{M}_i^{\text{out}}(t)}{dt} = X_i(t) \xi_i \frac{d\mathcal{M}_{\text{reheat}}(t)}{dt}, \quad (10)$$

where $X_i(t)$ is the abundance by mass of the element i in the ISM at the time t and $\mathcal{M}_{\text{reheat}}(t)$ is the ISM mass heated by SN explosions and ejected at the time t . ξ_i can be set to 1 for all elements (as in Li et al.'s 2010 paper) or to higher values for metals, to mimic a differential outflow.

Since the hypothesis of IRA is relaxed in our computations, our $\mathcal{M}_{\text{cold}}(t)$ value may differ from the corresponding SAM one (the differences are within a few per cent). Therefore, at each time step we readjust it to its SAM value. We do this after the gas mixture is assigned the proper chemical composition. It is worth stressing again here that the SAM may provide more than one value for $\mathcal{M}_{\text{cold}}(t)$ at each time step, depending on the number of progenitors. In order to deal with this, at each time step we sum up all the values of $\mathcal{M}_{\text{cold}}(t)$ from the SAM. The vast majority of such merging events occur in the early Universe in our models.

The inclusion of SNeIa and their delay times in the model has a huge impact on the predicted MDF and $[X/\text{Fe}]$ versus $[\text{Fe}/\text{H}]$ behaviour, as we will see in the next section.

3.3.3 Gas flows and star formation: the classical approach

For the purpose of comparison with the models computed within a cosmological framework, we also run a classical model for Sculptor. In the frame of such a model, a simple Schmidt (1963) star formation law is assumed, as usually done in classical chemical evolution studies:

$$\psi(t) = \nu \mathcal{M}_{\text{cold}}^k(t), \quad (11)$$

where ν and k are free parameters of the model, that are adjusted to reproduce the observations. The ν parameter is the star formation efficiency. It is related to ε , its counterpart in the SAM, through the relation $\nu = \varepsilon/t_{\text{dyn}}$, where t_{dyn} is the dynamical time and $\varepsilon = 0.03$ in the adopted SAM (see Sect. 3.2). Hence, the two quantities must not be directly compared. We do not consider a threshold gas density for star formation in the classic model. The raw material for star formation is accreted according to a time-decaying infall rate:

$$\frac{d\mathcal{M}_i^{\text{in}}(t)}{dt} = X_i^{\text{in}}(t) A e^{-t/\tau}, \quad (12)$$

with the accreted matter being usually assigned a primordial chemical composition, $X_i^{\text{in}}(t) = X_i^0$. The normalization constant, A , obeys the boundary condition

$$\int_0^{t_{\text{now}}} A e^{-t/\tau} dt = \mathcal{M}_{\text{acc}}, \quad (13)$$

where \mathcal{M}_{acc} is the total mass ever accreted by the system; t_{now} and τ are the age of the Universe and the infall time scale, respec-

Table 1. Properties of the ‘cosmological’ Sculptor galaxy models.

Model	$\mathcal{M}_{\text{stars}}$ ($10^6 M_{\odot}$)	$\mathcal{M}_{\text{cold gas}}$ ($10^6 M_{\odot}$)	$\langle [\text{Fe}/\text{H}] \rangle_{\text{stars}}$ (dex)	M_V (mag)
(1)	(2)	(3)	(4)	(5)
Scl1	6.1	2.2	$-0.9 (-1.6^a)$	-10.9
Scl2	2.7	14.	-1.7	-10.3
Scl3	4.3	0.1	$-1.1 (-1.5^a)$	-10.7
Scl4	13.	7.2	-1.4	-11.8
Observed ^b	~ 8.0	0.234	-1.9	-11.1

Note. Different columns list: (1) the model name; (2) the present-day stellar mass; (3) the present-day gaseous mass; (4) the mean metallicity of the stellar populations; (5) the V -band absolute magnitude. Observed values are given in the last row.

^aWith last star formation burst excluded.

^bThe stellar mass is estimated from the SFH of de Boer et al. (2012). The cold gas mass is the neutral hydrogen mass; notice the detection is ambiguous due to the numerous intervening clouds that could be mistaken for gas associated with Sculptor (Grcevich & Putman 2009). The mean stellar metallicity is computed from values in Table A1 of this work. The V -band absolute magnitude is obtained from the apparent magnitude reported by Irwin & Hatzidimitriou (1995), by assuming a distance of 86 kpc for Sculptor.

tively. We adopt $t_{\text{now}} = 13.8$ Gyr (cf. Bennett et al. 2012) for the present-day age of the Universe. SNe of all types inject energy in the surrounding ISM. When the thermal energy of the gas heated by SN explosions exceeds its binding energy, a galactic wind eventually develops. The rate of gas loss via galactic wind is

$$\frac{d\mathcal{M}_i^{\text{out}}(t)}{dt} = X_i^{\text{out}}(t) w_i \mathcal{M}_{\text{cold}}(t), \quad (14)$$

where $X_i^{\text{out}}(t) = X_i(t)$, namely, the abundance of each element in the wind is the same as in the ISM. The w_i terms are further parameters of the model that describe the efficiency of the outflow for each element; they are set all to the same value in the case of normal wind, but can take a higher value for metals in the case of differential, metal-enriched winds (Mac Low & Ferrara 1999; Recchi et al. 2001; Fujita et al. 2004).

In classical models, there is no distinction between cold and hot gas phases. The freshly produced metals are assumed to cool down in short time scales (i.e., shorter than the computation time steps) and $F = 0$ in equation (3). This means to have instantaneous mixing and instantaneous cooling of newly released metals in the models.

We set $\nu = 0.02 \text{ Gyr}^{-1}$, $k = 1$, $\mathcal{M}_{\text{acc}} = 1.7 \times 10^8 M_{\odot}$, $\tau = 5 \times 10^7 \text{ yr}$ and $w_{\text{H,He}} = 0.5 \text{ Gyr}^{-1}$, $w_{\text{metals}} \simeq 1 \text{ Gyr}^{-1}$. This is model Scl1. The parameters of this model have been tuned to reproduce, as best as we can within this simple working framework: (i) the CMDs (see de Boer 2012) and the detailed SFH of Sculptor inferred from observations (de Boer et al. 2012); (ii) the trends of several abundance ratios with $[\text{Fe}/\text{H}]$ in Sculptor’s stars; (iii) the MDF representative of the full Sculptor stellar population (see Appendix A) and (iv) the (likely) absence of neutral hydrogen in the galaxy at the present time (Grcevich & Putman 2009).

4 RESULTS

In this section we present our results concerning the detailed chemical composition of four Sculptor candidates selected by Starkenburg et al. (2013a) on luminosity ($-11.8 < M_V < -10.3$) and

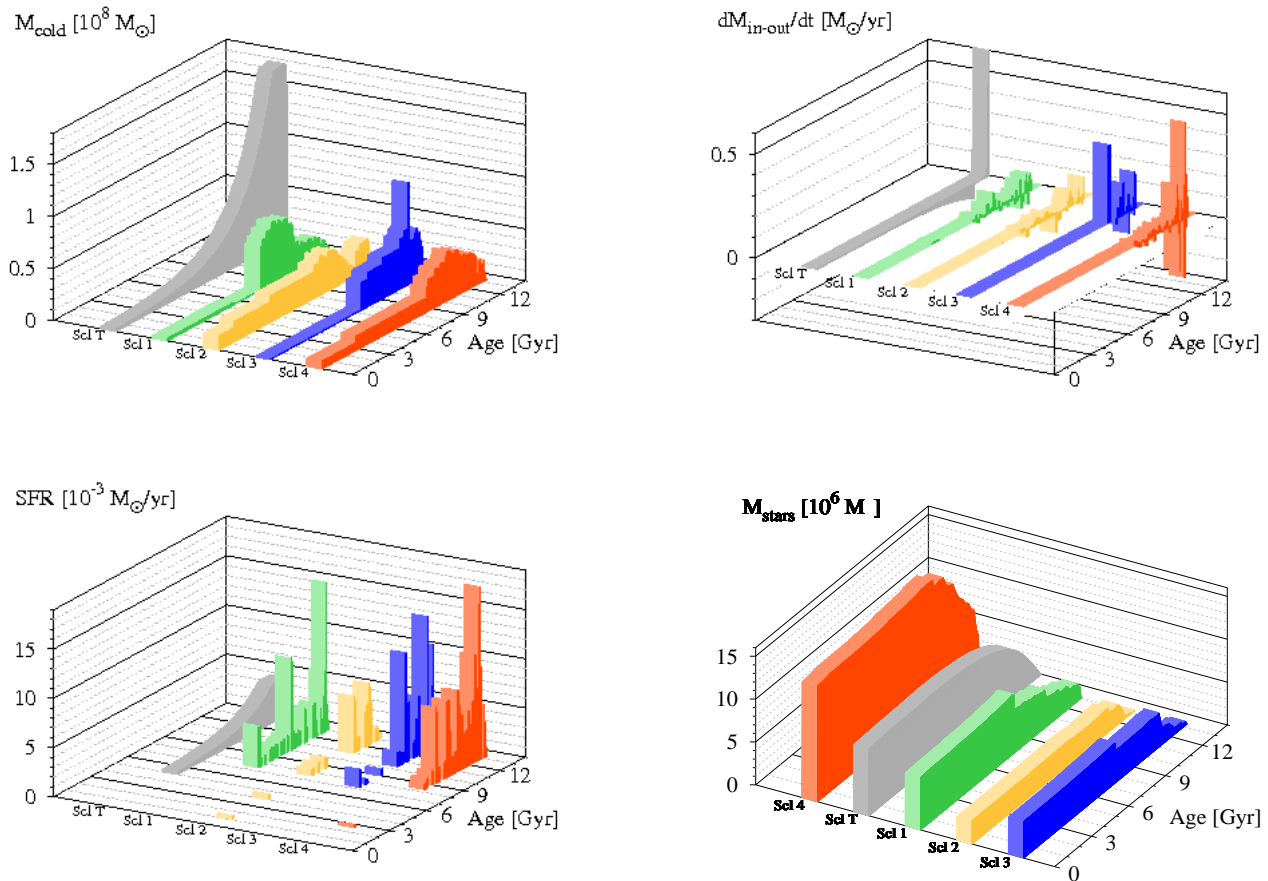


Figure 2. Counterclockwise from top left: evolution of the cold gas masses, SFRs and cumulative stellar masses for models Scl T (grey walls), Scl 1 (green walls), Scl 2 (yellow walls), Scl 3 (blue walls) and Scl 4 (red walls). In the top right box we show the difference between incoming and outgoing cold gas fluxes for the same models.

dominant old stellar population criteria. The outputs of these ‘cosmologically motivated’ models are compared to the ones from a classical model, as well as to the relevant data. All the theoretical abundance ratios discussed in this work are normalized to the solar abundances by Grevesse & Sauval (1998).

In Fig. 2 we show the evolution of the cold gas masses, the net change in cold gas masses, the SFRs and the cumulative stellar masses for the four models listed in Table 1. The cold gas masses, gas flows and SFRs are the input of the post-processing code described in the previous section. A classical model of chemical evolution meant to meet the main observational constraints for Sculptor (see Sect. 3.3.3) is considered as well (Fig. 2, grey walls).

It is immediately seen (Fig. 2, top left box) that, at early evolutionary stages, a gross cold gas amount, of more than $1.5 \times 10^8 M_{\odot}$, characterizes the classical model, which leaves behind a small stellar system of only $M_{\text{stars}} = 7.8 \times 10^6 M_{\odot}$ (Fig. 2, bottom right box). In contrast, in hierarchically growing systems a much lower (up to one order of magnitude) cold gas mass is predicted at early epochs. Yet, the current stellar masses are in between 2.7 and $13 \times 10^6 M_{\odot}$, reflecting a more efficient star formation in these models. Another striking difference regards the history of mass assembly. While in the classical approach it is fairly simple—a short phase of strong gas accretion, followed by a much longer period in which mass loss dominates—the models computed within the

hierarchical scheme of galaxy formation display far more complex patterns (see Fig. 2, top right box). Because of the assumed critical density threshold for star formation, the SFR of the cosmological models may be zero even if the gas content is different from zero (Fig. 2, bottom left box). Model Scl 2 predicts a present-day cold gas mass significantly higher than the limit on the neutral hydrogen mass suggested by Grevech & Putman (2009) for the Sculptor dSph (Table 1). Therefore, it can be ruled out as a good Sculptor replica. Also Model Scl 4 predicts a present-day cold gas mass higher than observed.

It is worthwhile mentioning here that, while the adopted SAM reproduces the luminosity function of Milky Way’s satellites well, the predicted stellar mass versus dark matter halo mass relation is offset with respect to the extrapolations of the Guo et al. (2010) and Moster et al. (2010) abundance matching relations (but it is in accordance with hydrodynamical simulations; see Starkeburg et al. 2013a).

4.1 Age-metallicity relation and metallicity distribution function

At early times, because of the lower amounts of diluting gas the models computed within the hierarchical picture for structure formation typically reach higher metallicities than the classical one.

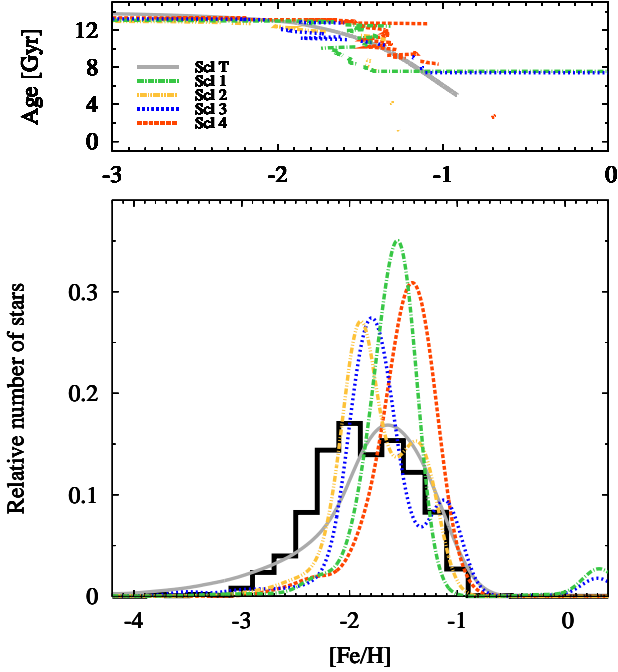


Figure 3. Age-metallicity relations (upper panel) and MDFs (bottom panel) for our model galaxies Scl 1 (green dot-dashed lines), Scl 2 (yellow dot-dot-dashed lines), Scl 3 (blue dotted lines), Scl 4 (red dashed lines) and Scl T (grey solid lines). The theoretical MDFs have been smoothed by a Gaussian function with a variance equal to the data error, 0.15 dex. The black solid histogram is the observational MDF we obtain by combining the DART CaT sample (Battaglia et al. 2008b; Starkenburg et al. 2010) with the sample by Kirby et al. (2010), as specified in Appendix A.

This is clearly seen in Fig. 3, upper panel, which displays the age-metallicity relations of all our model galaxies. Model Scl 2 is a notable exception, in that it has the smoothest metallicity increase during the first Gyr of evolution, due to its low-level star formation at those old ages. The abrupt rise in metallicity characterizing models Scl 1 and Scl 3 at an age of ~ 7.5 Gyr (the horizontal portions of the green dot-dashed and blue dotted lines, respectively, on the right in Fig. 3, upper panel), is due to the last, strong bursts of star formation, that almost exhaust the cold gas in these model galaxies (Fig. 2, green and blue walls, bottom and top left boxes).

In Fig. 3, upper panel (as well as in all the following figures of this paper), some gaps appear in the theoretical curves for models Scl 1, Scl 2, Scl 3 and Scl 4. They arise because we do not plot the portions of the curves that correspond to halts in star formation (the curves reflect the chemical composition of the ISM at each time; if the SFR at that time is zero, no stars form with the corresponding chemical composition). For the same reason, the curve relative to model Scl T ends at an age of 5 Gyr, i.e. when the star formation is stopped in this model. We impose a cut-off time for star formation in model Scl T to better match the SFH of Sculptor derived by de Boer et al. (2012). However, it is worth emphasizing that the star formation activity in model Scl T is fading at ages less than 5 Gyr and would die out anyway because of the strong mass loss through the outflow and scarce replenishment of gas from outside.

An important diagnostic to test our models is the MDF of long-lived stars, which allows us to fine-tune some important parameters regarding chemical evolution (see Sect. 4.3 for a thorough discussion). In Fig. 3, bottom panel, our theoretical MDFs

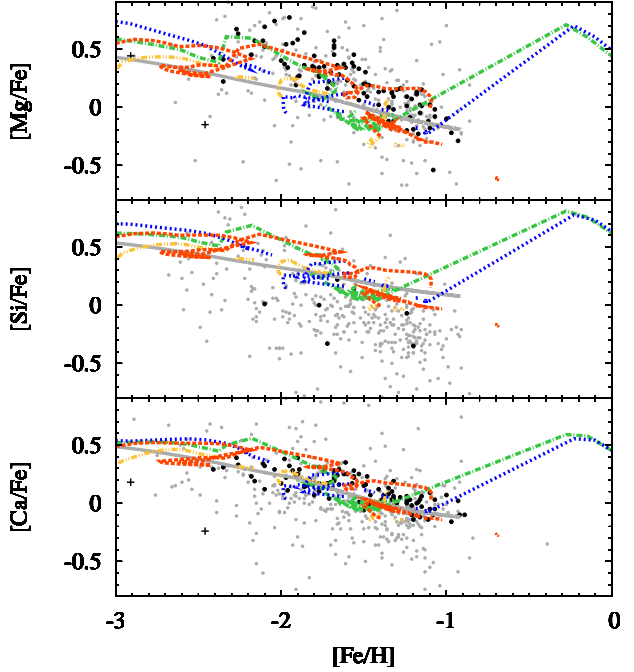


Figure 4. $[X/Fe]$ versus $[Fe/H]$ for several α -elements (Mg, Si and Ca) predicted by models Scl 1 (green dot-dashed lines), Scl 2 (yellow dot-dot-dashed lines), Scl 3 (blue dotted lines), Scl 4 (red dashed lines) and Scl T (grey solid lines). The grey dots represent the data from medium-resolution spectra by Kirby et al. (2009), the black dots those from high-resolution spectra by Shetrone et al. (2003, 5 stars), Geisler et al. (2005, 4 stars) and Hill et al. (in preparation, 89 stars; see Tolstoy et al. 2009). Data from Starkenburg et al. (2013b) are shown as crosses.

(lines) are compared to the observational one (solid histogram; see Appendix A). The theoretical MDFs have been convolved with a Gaussian ($\sigma = 0.15$) to take the observational errors into account. Model Scl T successfully reproduces the existence of stars with $-4 < [Fe/H] < -2.5$ in the right percentage (by construction), but the number of very metal-poor stars in the metallicity range $-2.5 < [Fe/H] < -2$ is underestimated by about 25 per cent. The ‘cosmological’ models severely underestimate the number of very metal-poor stars[§]. Models Scl 2 and Scl 3 show a prominent peak at $[Fe/H] \sim -1.9$ dex, in fairly good agreement with the observations, but predict unwanted secondary peaks at higher metallicities as well. The last, intense bursts of star formation closing the SFHs of models Scl 1 and Scl 3 produce small fractions of stars (about 5 per cent of the total) with supersolar metallicities, that have no match in the real galaxy. According to models Scl 1, Scl 2, Scl 3 and Scl 4, basically no stars are expected below $[Fe/H] \simeq -2.5$ dex. In this context, a detailed implementation of the formation of the first stars would be an interesting addition to the current SAM. Implementation of those physical processes could potentially alter the

[§] We note that, while in the adopted SAM many Sculptor analogs are found when looking at the SFH—most model satellites are dominated by stars formed at old ages—candidates of comparable luminosity tend to have slightly higher average metallicity than Sculptor (Starkenburg et al. 2013a). This is in qualitative agreement with observations of dwarf galaxies, using the luminosity and metallicity as quoted in this paper the Sculptor dSph is placed on the lower edge of the observed scatter in the luminosity-metallicity relation.

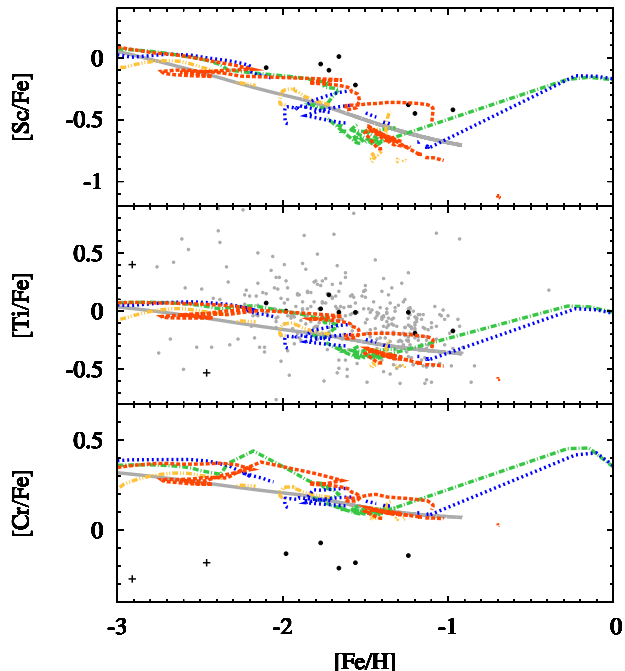


Figure 5. Same as Fig. 4, for Sc, Ti and Cr.

first phases of star formation in the dwarf galaxies and, hence, alter the MDF at the very metal-poor end. We also note that a lowering of the initial mass limit for black hole formation in stellar populations of very low-metallicity would result in a diminished production of iron during early galactic evolution (more heavy elements would be swallowed by black holes in this case; cf. Maeder 1992; Woosley & Weaver 1995), thus leading to a better fit of the very low-metallicity tail of the MDF.

4.2 Abundance ratios

In Figs. 4 to 6 we show our model predictions on the $[\text{X}/\text{Fe}]$ versus $[\text{Fe}/\text{H}]$ behaviour for several α and iron-peak elements in the stars of Sculptor. The model predictions are compared to data from high- and medium-resolution spectra of giant stars in Sculptor (see Sect. 2 and figure captions for references). Data for a few stars below $[\text{Fe}/\text{H}] = -3$ dex seem to point to a non-negligible dispersion which, in turn, would point to inhomogeneous chemical evolution in the early galaxy. Since currently our model is not able to deal with chemical inhomogeneities, we restrict our comparison to the metallicity range $-3 < [\text{Fe}/\text{H}] < -0.8$. All abundance ratios are normalized to solar values by Grevesse & Sauval (1998), apart from Kirby et al. (2009) and Shetrone et al. (2003), who use $\log(N_{\text{Fe}}/N_{\text{H}}) = 7.52$ rather than 7.50 for the solar abundance of iron, and Geisler et al. (2005), who adopt $\log(N_{\text{O}}/N_{\text{H}}) = 8.77$ rather than 8.83 for the solar abundance of oxygen. These differences of a few hundredths of dex are smaller than quoted uncertainties of the measurements and were therefore neglected.

The ratio of α elements to iron is commonly believed to be a powerful tracer of the timescale of formation of a stellar system, because of its sensitivity to the ratio of short-lived SNIi to long-lived SNIa progenitors. During the earliest stages of the evolution, basically only SNIi contribute to the chemical enrichment and, thus, high $[\alpha/\text{Fe}]$ ratios are observed. As soon as SNIa start to domi-

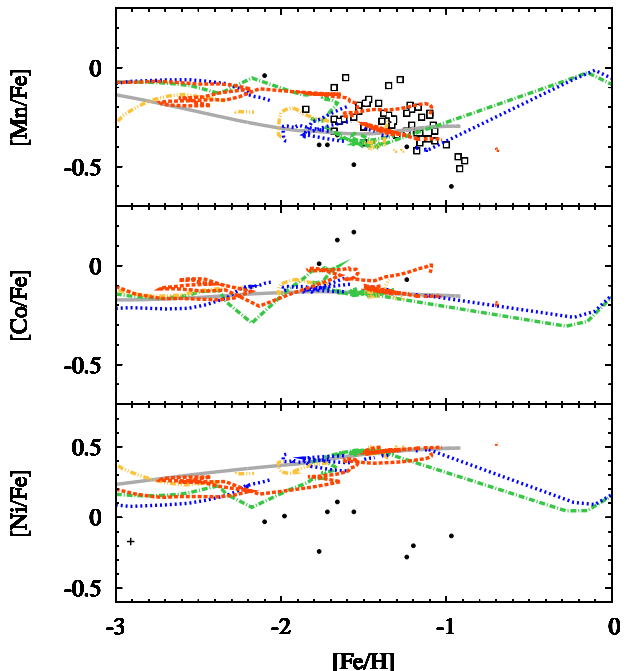


Figure 6. Same as Fig. 4, for Mn, Co and Ni. Open squares (top panel) are data from North et al. (2012).

nate the iron production, a ‘knee’ is produced in the $[\alpha/\text{Fe}]$ versus $[\text{Fe}/\text{H}]$ plot (Matteucci 2001, and references therein). Galaxies with low SFRs and/or that lose their metals in a galactic wind will show (more or less clearly) the knee at metallicities lower than galaxies with high SFRs that retain their metals. Of particular interest as probes of the enrichment timescales are also those elements whose yields are highly dependent on the metallicity of the parent stars, such as manganese (Romano et al. 2011, and references therein).

Owing to its bursting star formation mode, with few short active phases separated by long quiescent periods (see Fig. 2, bottom left box, yellow wall), model Scl2 displays the most ‘scrappy’ lines in Figs. 4 to 6, with many gaps in $[\text{Fe}/\text{H}]$: the abundance of Fe, that is produced mainly by SNIa on long timescales, continues to grow in the ISM even if the star formation goes to zero, unless the accretion of a substantial amount of metal-poor matter dilutes the enriched medium. An important accretion of nearly unprocessed gas actually happens several times in the evolution of model Scl4 (notice the numerous right-to-left shifts in the path followed by this model in Figs. 4 to 6). Overall, our models are in reasonable agreement with the abundance data for Sculptor, especially if considering that the yields of Sc and Ti from massive stars are underestimated, while those of Cr are overestimated, in the metallicity range probed by this study and that current SNIa models do highly overestimate the production of Ni (see Romano et al. 2010a, and references therein). In particular, model Scl4 is in excellent agreement with the high-resolution data for Mg in Sculptor (Fig. 4, top panel) and nicely reproduces the striking decreasing trend of $[\text{Mn}/\text{Fe}]$ versus $[\text{Fe}/\text{H}]$ found in this galaxy (North et al. 2012; see Fig. 6, top panel).

For the α -element magnesium, model Scl1 (green dot-dashed line in Fig. 4, upper panel) predicts a knee steeper than suggested by the high-resolution data in the $[\alpha/\text{Fe}]$ versus $[\text{Fe}/\text{H}]$ plot, while model Scl7 produces a curve that is too flat (grey solid line in Fig. 4, upper panel). Since all model galaxies presented in this

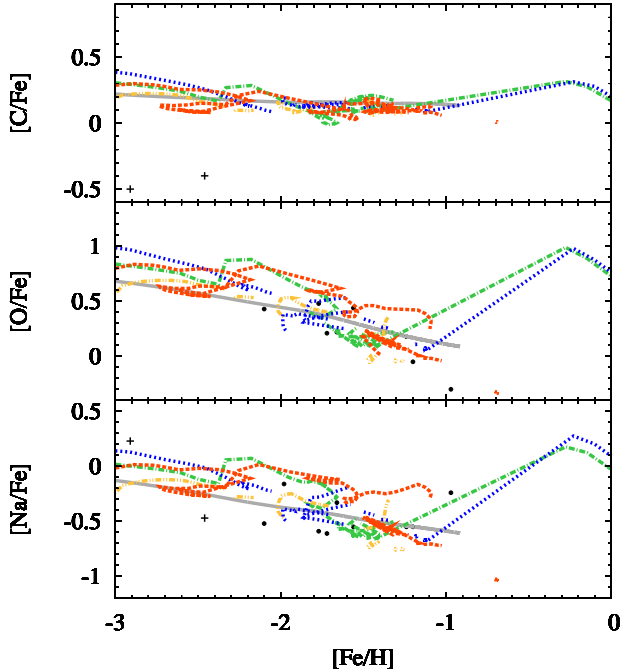


Figure 7. Same as Fig. 4, for C, O and Na.

work share the same prescriptions about SNIa progenitors and nucleosynthesis (see Sect. 3.3.1), we conclude that the specific histories of star formation and mass assembly play a crucial role in determining the exact shape of the $[\text{Mg}/\text{Fe}]$ – $[\text{Fe}/\text{H}]$ (and $[\text{Mn}/\text{Fe}]$ – $[\text{Fe}/\text{H}]$) relation in Sculptor.

As already mentioned, at the lowest metallicities, $-4 < [\text{Fe}/\text{H}] < -3$, the data show a significant dispersion. Stochastic sampling of the IMF as a consequence of the low SFRs (Carigi & Hernandez 2008; Cescutti 2008) may be, at least partly, responsible for the observed scatter. Our model does not incorporate yet inhomogeneous mixing of pockets of gas which are enriched by a certain type of SN event. However, there is increasing evidence that such inhomogeneous mixing exists in the early generations of star formation in dwarf galaxies (e.g. Tafelmeyer et al. 2010; Venn et al. 2012). In the data set of very metal-poor Sculptor stars of Starkenburg et al. (2013b), one star shows low α - and heavy elements compared to iron. This is consistent with a picture in which the star was born from a SNIa enriched pocket (Marcolini et al. 2006). A stronger case of such a star was discovered in the Carina dwarf galaxy (Venn et al. 2012). Efforts are ongoing to include inhomogeneous mixing in our chemical evolution code.

In Fig. 7 we show, from top to bottom, our predictions for $[\text{C}/\text{Fe}]$, $[\text{O}/\text{Fe}]$ and $[\text{Na}/\text{Fe}]$ versus $[\text{Fe}/\text{H}]$ in Sculptor. These predictions need to be confirmed (or disproved) by future observations. In fact, only sparse data are available at present for these elements. As for carbon, we caution that in giant stars dredge-up of CNO-processed material to the surface may expose C-poor, N-rich matter and complicate the interpretation of the abundances (Spite et al. 2005).

4.3 Major model uncertainties

Up to now, we have compared the outputs of different models for Sculptor—a classical, ‘non-cosmological’ one (model labelled

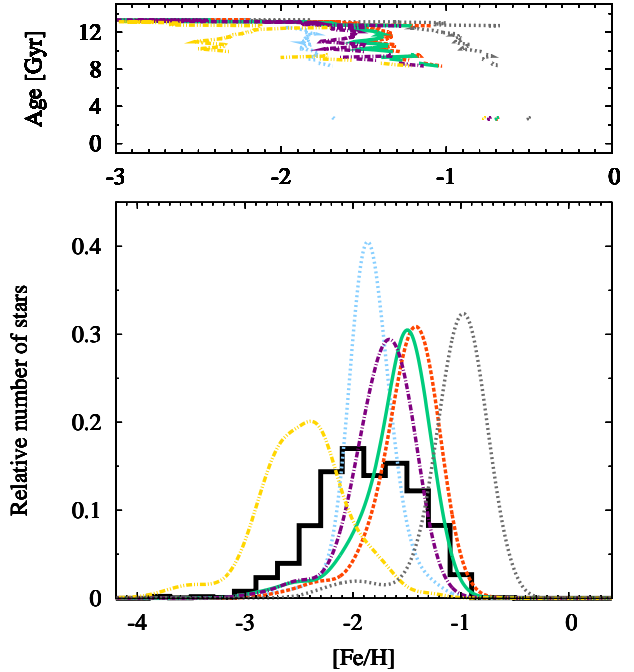


Figure 8. Age-metallicity relations (upper panel) and MDFs (bottom panel) obtained with model Scl4 with different prescriptions about the IMF or the metal losses (yellow dot-dot-dashed, purple dot-dashed, green solid, red dashed and grey dotted lines; see text) or without including the contribution of SNeIa to the stellar nucleosynthesis (sky-blue dotted lines). The theoretical MDFs have been smoothed by a Gaussian function with a variance equal to the data error, 0.15 dex. The black solid histogram is the observational MDF we obtain by combining the DART CaT sample (Battaglia et al. 2008b; Starkenburg et al. 2010) with the sample by Kirby et al. (2010), as specified in Appendix A.

SclT) and four ones based on full cosmological simulations (models labelled Scl1, Scl2, Scl3 and Scl4). The values of the parameters for model SclT are listed in Sect. 3.3.3; they are fixed mainly by the requirement of reproducing the SFH of Sculptor inferred from the observations (de Boer et al. 2012), as well as its stellar MDF (this work, Appendix A). As for models Scl1, Scl2, Scl3 and Scl4, the results that we present in Sects. 4.1 and 4.2 rest on the following assumptions: (i) the hot ejecta of SNe of all types cool and mix with the ISM on short time scales (i.e., shorter than the typical time step for computation); (ii) the metals heated by SN explosions and entrained in the outflow never re-enter star formation in the system; (iii) the realization probability for SNIa events is the same as in our Galaxy. To conclude our inspection of Sculptor-like model galaxies, we show in the following how the predictions of model Scl4 change when modifying these standard assumptions. Furthermore, we quantify the effects of small variations in the IMF slope.

4.3.1 The role of SNeIa

In Figs. 8 and 9, we show the predictions concerning the age-metallicity relation, MDF and $[\text{X}/\text{Fe}]$ versus $[\text{Fe}/\text{H}]$ behaviour (for Mg, Ca and Mn; we select only elements with both reliable nucleosynthesis prescriptions and homogeneous measurements from high-resolution spectra in a large number of stars) of model Scl4 computed including the contribution from SNeIa (red dashed lines; standard choice) and without SNeIa (sky-blue dotted lines). It is

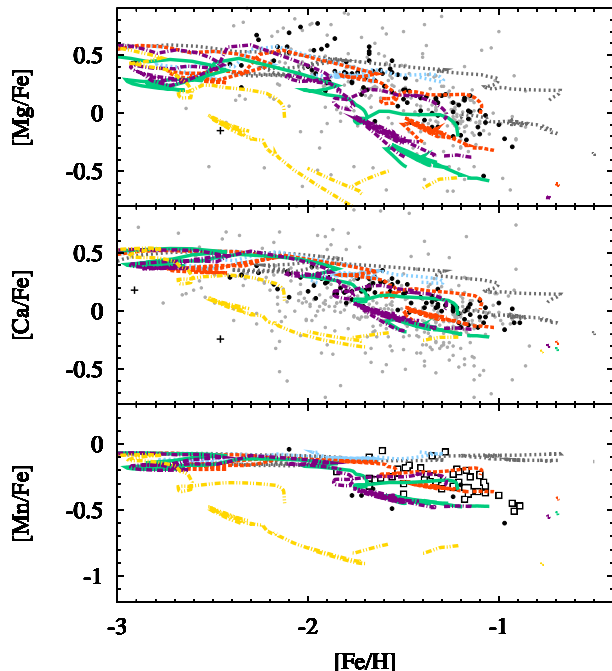


Figure 9. $[X/Fe]$ versus $[Fe/H]$ relations for Mg, Ca and Mn in Sculptor. The predictions of model Scl4 with different prescriptions about the IMF or the metal losses, or without including SNeIa nucleosynthesis (lines, see text and caption to Fig. 8) are displayed and compared to the relevant data (symbols, see Sect. 2 and captions to Figs. 4 and 6 for references).

immediately seen that without SNeIa the predicted MDF peaks towards lower metallicities, in better agreement with the observed one, but it narrows as well, at variance with the observations. Furthermore, without SNeIa there is no knee in the $[\alpha/Fe]$ versus $[Fe/H]$ plot and the observed decrease of $[Mn/Fe]$ for $[Fe/H] > -1.5$ dex is not reproduced any more. Clearly, SNeIa are of primary importance to reproduce the chemical features of stars in Sculptor. This result is not new —it has been shown several times in the literature that SNeIa are required in order to accurately reproduce the chemical compositions of galaxies. Nevertheless, we deem worth showing here the results of model Scl4 computed without SNeIa, to make it clear that the lack of very metal-poor stars below $[Fe/H] = -2.3$ dex, plaguing all of our cosmologically-motivated models for Sculptor (see Fig. 3, lower panel) is almost unrelated to the number of prompt SNeIa exploding in the models (see Fig. 8, lower panel; red dashed versus sky-blue dotted lines). Our failure in reproducing the very low-metallicity tail of the observed MDF would rather point to the need for more diluting gas and/or a more efficient sink for metals during the earliest phases of galaxy evolution.

We stress here that, while in our post-processing code the contribution of SNeIa to the nucleosynthesis is taken into account in detail (see Sect. 3.3.1), in the adopted SAM SNeIa are not included, either in the metal or energy budgets. Since their contribution to feedback processes in galaxies may become important as well, especially during the late stages of the evolution in case of protracted star formation (e.g. Bradamante et al. 1998; Recchi et al. 2001), we caution that the results presented in this paper could change when a detailed treatment of SNIa feedback is included in the SAM.

4.3.2 The role of the IMF

Throughout this paper, we adopt an extrapolation of the Salpeter (1955) IMF, defined in the mass range $0.1\text{--}100 M_{\odot}$. This is a common choice in chemical evolution studies. However, in order to investigate the stability of our results against (plausible) IMF variations, we also run model Scl4 by assuming a Chabrier-like IMF normalized to unity in the $0.001\text{--}100 M_{\odot}$ mass range and with $x = 1.7$ in the exponential law for $m > 1 M_{\odot}$ ($x = 1.35$ for Salpeter).

We note that in the original paper, Chabrier (2003) quotes $x = 1.3 \pm 0.3$ to take the observational errors into account. Here we adopt an extreme —but still empirically supported (see Kroupa 2001, 2012)— value for the IMF slope. We do this in order to maximize the differences in the model outputs with respect to our standard (Salpeter) choice. With our particular choice of a Chabrier-like IMF, the predicted MDF shows a negligible shift towards lower $[Fe/H]$ values (green solid versus red dashed lines; Fig. 8, bottom panel). The predicted $[X/Fe]$ ratios are lowered (green solid versus red dashed lines; Fig. 9), but the effect is noticeable (~ 0.3 dex at maximum) only for the elements originating mostly from SNeII, such as Mg.

Overall, reasonable changes in the IMF produce secondary-order effects on the predicted MDF of our model galaxies (see also Marconi et al. 1994). However, the predicted abundance ratios may vary significantly, depending on the elements.

4.3.3 The role of metal recycling through the hot phase

Following Li et al. (2010) and Starkeburg et al. (2013a), models Scl1, Scl2, Scl3 and Scl4 include a route to recycle the metals produced by dying stars through the hot phase of a galaxy. In our standard model, a substantial fraction [$F = 0.95$ in equation (3)] of metals is ejected directly into the hot gas component and can be reincorporated in the cold gas phase later on (the remainder goes directly in the cold phase). Here we investigate further this assumption by studying two extreme cases: (i) SN ejecta put in the hot phase are directly available for cooling again; (ii) SN ejecta are subtracted from the cold gas phase forever. The yellow (dot-dot-dashed) lines in Figs. 8 and 9 show the predictions of model Scl4 in case the metals deposited in the hot phase are made to never re-enter regions of active star formation, compared to the case in which they are immediately and fully reincorporated (standard choice, red dashed lines). In case of inefficient metal recycling, the peak of the theoretical MDF shifts towards lower metallicities and the distribution broadens. One might be, thus, led to believe that the best-fitting solution involves some fine tuning, with large fractions of the newly-produced metals deposited directly in the hot gas phase never getting back to regions of active star formation. However, a glance at Fig. 9 (yellow dot-dot-dashed versus red dashed lines) reveals that, in order to honour the constraints imposed by the trends of the abundance ratios with metallicity, most of the stellar ejecta must instead cool and mix with the neutral ISM forming the next generations of stars!

Apart from the injection of freshly produced metals from dying stars directly in the hot component, another mode of metal removal from the star-forming regions is active in our models, i.e. entrainment of (part of) the ISM perturbed by SN explosions in the outflow [this is the ejected gas component, see Fig. 1; see also Sect. 3.3.2, equation (10)]. In our standard scheme, the metals carried away by the outflow are assumed to be definitively lost from the system. If, instead, they are fully recycled through the hot gas

phase, the theoretical MDF is found to span the metallicity range $-2.5 < [\text{Fe}/\text{H}] < -0.5$ with a peak at $[\text{Fe}/\text{H}] -1.0$ dex, at variance with the observations; furthermore, the knees in the theoretical $[\alpha/\text{Fe}]-[\text{Fe}/\text{H}]$ relations are shifted towards higher metallicities and flatter relations are predicted (grey dotted lines in Figs. 8 and 9). This is because the system can reach higher metallicities by the time SNeIa start to contribute the bulk of their Fe to the ISM. Finally, the purple (dot-dashed) curves in Figs. 8 and 9 refer to model Scl 4 computed by assuming $\xi_i = 1$ for H and He and $\xi_i = 2$ for metals in equation (10) (in the standard case, red dashed lines, we set $\xi_i = 1$ for all elements). This choice is the analogous to the differential, metal-enriched wind hypothesis in classical chemical evolution studies. With this choice, the peak of the distribution shifts towards lower metallicities, but the model barely matches the available abundance data. Setting ξ_i to even higher values for metals results in unacceptable theoretical $[\text{X}/\text{Fe}]$ versus $[\text{Fe}/\text{H}]$ relations: in fact, the knee in the $[\alpha/\text{Fe}]$ versus $[\text{Fe}/\text{H}]$ plot moves to $[\text{Fe}/\text{H}] < -2.3$ dex, at variance with the observations, and a slope steeper than observed is obtained for $[\text{Fe}/\text{H}] > -2$ dex (models not shown in Figs. 8 and 9, to avoid overcrowding).

Summarizing: Accretion of pristine—or nearly unpolluted—gas, either through infall or ingestion of small, gas-rich satellite systems, and subsequent conversion of this gas into stars play a fundamental role in determining the final chemical properties of galaxies. Having fixed the histories of mass accretion and star formation by means of cosmological simulations and a SAM of galaxy formation, the results presented in this work are largely driven by the amount of metals that the galaxy is able to lose—or, better, to subtract from the cold, star-forming phase—at any time, *as well as to the mode of the metal losses*. Indeed, it makes a difference if the SN ejecta are vented out of the galaxy directly, i.e. without interacting with the surroundings, or if some mixing with the ambient medium is permitted before. We prefer a scenario in which a significant dilution does occur: the simultaneous comparison of our model results with both a well-defined observational MDF and high-quality abundances in a large sample of stars allows us to significantly constrain the parameter space of the model and to discriminate among different possible evolutive scenarios.

5 DISCUSSION

The idea of substantial mass loss on a galactic scale from starbursts in small galaxies is not new. In particular, the existence of differential winds, i.e. galactic winds in which heavier elements are vented out of the galaxy more efficiently than lighter ones, was first hypothesized and applied to the chemical evolution of generic dwarf galaxies by Pilyugin (1993). Shortly after, Marconi et al. (1994) introduced the concept of *selective winds*, i.e. differential winds in which different metals have different ejection efficiencies in dependence on the nature of the parent stars (see also Recchi et al. 2001; Fujita et al. 2004; Romano et al. 2010b). Nowadays, metal-enriched outflows are often invoked by modellers to reproduce the observed metallicity-luminosity relation of dwarf galaxies, as well as detailed abundance data for specific objects, in the context of both classical chemical evolution studies (e.g. Carigi et al. 2002; Lanfranchi & Matteucci 2003, 2004; Romano et al. 2006; Yin et al. 2011) and *ab initio* galaxy formation models (e.g. Salvadori et al. 2008; Calura & Menci 2009; Sawala et al. 2010). In the following, we discuss our findings in comparison to recent theoretical studies dealing with the Sculptor dSph.

In their numerical chemical evolution model for Sculptor,

Lanfranchi & Matteucci (2003, 2004) have adopted the SFH inferred from the CMDs (Dolphin 2002) and imposed that the metals produced by SNe of all types are efficiently removed by strong differential galactic winds. Notwithstanding this, their Sculptor gets too rapidly relatively metal-rich and the theoretical MDF (Lanfranchi & Matteucci 2004, their figure 6) completely lacks the most metal-poor stars observed in Sculptor. In our ‘cosmological’ models, we similarly miss the stars with $[\text{Fe}/\text{H}] < -2.5$ dex (this work, Fig. 3, lower panel). However, the shape of the $[\text{Mg}/\text{Fe}]$ versus $[\text{Fe}/\text{H}]$ relation predicted by both Lanfranchi & Matteucci (2004, their figure 3) and ourselves (this work, Fig. 4, upper panel) agrees very well with observations of giant stars in Sculptor. We also note that in Lanfranchi & Matteucci’s study the ratio of α -elements to Fe in the ISM of Sculptor is predicted to monotonically decrease in time (see also the results of our classic model, grey lines in Fig. 4). This is essentially due to the monotonic behaviour of the assumed accretion rate of pristine gas for star formation, leading to a one-to-one age-metallicity relation for Sculptor. Our ‘cosmological’ models, instead, display more complicated AMRs, because of the much more complex histories of mass assembly predicted by the underlying SAM. Thus they predict, within a given galaxy, the existence of stars with the same metallicity, but with different ages and, hence, with different abundance ratios. This can explain a moderate degree of inhomogeneity (up to 0.3 dex) in the data. Models Scl 1 and Scl 3 also interestingly predict that in a minority of metal-rich stars with $[\text{Fe}/\text{H}] > 0$ dex, the abundance ratios are reset to the values reflecting type II SN nucleosynthesis. This happens because of the strong star formation bursts that end the evolution of these model galaxies some 8 Gyr ago (see Fig. 2): the gas is almost exhausted, the chemical imprints of previous galactic evolution are washed out and we just see the preponderant signature of the latest numerous core-collapse SNe. Although, actually, no stars with $[\text{Fe}/\text{H}] > -0.8$ dex are observed in Sculptor. In the case of model Scl 3, the last burst occurs after the galaxy has become a satellite, in which case the physics of star formation has become even more uncertain to predict—it is, therefore, unclear if we can exclude these model galaxies as good representatives of the Sculptor dwarf spheroidal on the basis of a very small population originating in one particular event. The mechanism discussed above is interesting as it could, in principle, explain the existence of a Mg-rich population at intermediate ages, as observed in the Carina dwarf galaxy (Lemasle et al. 2012). We plan to deal with the Carina dSph, as well as other well-studied dwarf galaxies of the Local Group, in a forthcoming paper of this series.

More recently, Kirby et al. (2011a) have readdressed the issue of the chemical evolution of Sculptor in the light of their new data and discussed some simple analytic models for Sculptor, tailored to reproduce the observational MDF they present elsewhere (Kirby et al. 2009, 2010). The low-metallicity tail of the observed distribution is reproduced by their simple models, but the peak of the theoretical distributions is located at $[\text{Fe}/\text{H}] = -1.6$. This is in reasonable agreement with the MDF derived from observations of stars in the inner $\sim 0.2^\circ$ region of Sculptor (Kirby et al. 2009, 2010), but in poorer agreement with the MDF representative of the full Sculptor galaxy derived in this paper (see Appendix A). Overall, their theoretical MDFs are quite similar to the one we obtain in the framework of the classical chemical evolution model discussed in this work (model labelled Scl T in previous sections).

In general, it seems difficult to reproduce the correct fraction of stars with $-2.5 < [\text{Fe}/\text{H}] < -1.5$ observed in Sculptor, and this problem pertains to both classical and ‘cosmological’ models. Possible solutions include: (i) the implementation of Population III

stars (with highly uncertain yields and IMF) in the models; (ii) a favoured black hole formation as the outcome of massive star evolution at low metallicities (with consequent sink of metals); (iii) a lower rate of occurrence of SNIa events at low metallicities (and/or in dense systems) and (iv) assembly from small subunits where the star formation is strongly suppressed in the early stages of galaxy evolution. In a forthcoming paper (Romano et al., in preparation), we will deal with points (i) to (iii). Points (i), (ii) and (iv) also provide possible solutions to the problem of the low fractions of stars below $[\text{Fe}/\text{H}] = -2.3$ dex predicted by models Scl1, Scl2, Scl3 and Scl4. Revaz & Jablonka (2012) obtain a better fit to the low-metallicity wing of the observed Sculptor MDF (as well as a good fit to the observed $[\text{Mg}/\text{Fe}]$ versus $[\text{Fe}/\text{H}]$ relation) through a smoothed particle hydrodynamics code. Yet, their Sculptor model needs to have its star formation artificially stopped. Moreover, it retains a large amount of gas, $\mathcal{M}_{\text{cold gas}} = 1.9 \times 10^7 M_{\odot}$ at the present time, to be compared with values one to two orders of magnitude lower for most of our models (see Table 1, third column). On the observational side, Grcevich & Putman (2009) have shown that $\mathcal{M}_{\text{HI}} = 2.34 \times 10^5 M_{\odot}$ of neutral hydrogen are possibly associated to the Sculptor dSph, but the detection is ambiguous.

Based on their modelling, Kirby et al. (2011b) have estimated that Local Group dSphs have lost from 96 to more than 99 per cent of the metals their stars manufactured. They suggest that gas outflows carried away most of the metals produced by these dSphs. For the post-starburst galaxy NGC 1569, there is indeed direct evidence (from X-ray spectral fit to several α elements; Martin et al. 2002) that the galaxy is losing nearly all of the metals it has produced in the latest starburst. However, three-dimensional hydrodynamic simulations by Marcolini et al. (2006) exclude that local dSphs got rid of their gas by internal mechanisms such as galactic winds. According to those authors, the evolution towards gas-poor systems would result from external mechanisms (ram pressure stripping and/or tidal interactions with the Milky Way). In their models, the SN ejecta remain gravitationally bound to the parent system. Yet, only a small fraction (less than 18 per cent) of it lies in the region where the star formation is active, which avoids the production of metal-rich stars. In Marcolini et al.’s (2006) simulations, the knee in the $[\alpha/\text{Fe}]$ versus $[\text{Fe}/\text{H}]$ diagram is due to the inhomogeneous distribution of the SNIa ejecta, rather than to the combined effect of the time delays with which SNeIa restore the bulk of their iron to the ISM and the onset of a galactic wind, as in classical chemical evolution studies (and this work). However, a significant scatter in the $[\text{O}/\text{Fe}]$ ratios is predicted at relatively high metallicities, that is not confirmed observationally. In fact, high-resolution spectroscopic data—and medium-resolution data, taking into account the larger uncertainties in these data—for hundreds of stars in Sculptor point rather to a remarkable homogeneity of the ISM during most of the evolution of the system (Kirby et al. 2009, 2010; Tolstoy et al. 2009; North et al. 2012; Hill et al., in preparation).

In the works by Li et al. (2010) and Starkenburg et al. (2013a), the following feedback scheme is adopted: (i) 95 per cent of SN ejecta goes directly into the hot gas phase (the remainder 5 per cent instantly pollutes the neutral ISM); (ii) metals in the ISM perturbed by SN explosions are put in an ejected component; they can re-enter the cold gas phase if recycled through the hot gas. In our models, we assume the cooling flow (grossly, H plus He) dictated by the cosmological simulations and SAM. The metallicity of the flow is further investigated: (i) SN ejecta in the hot gas are either put all straight into the cold gas phase (standard choice) or made never enter the cold gas phase; (ii) metals in the ejected component are either definitively lost from the system (standard choice) or fully

recycled through the hot gas phase. Our standard scheme, namely the one in which SN ejecta mix instantaneously with the surrounding ISM, but the metals in the ejected component are lost, does not have a physical motivation. But we do find that it reproduces the observed chemical properties of Sculptor’ stars. Full hydrodynamical simulations are needed in order to deal properly with issues such as the interaction of the metal-rich matter processed by the starburst with the ambient medium and the metal losses from the galaxy (see Recchi & Hensler 2013, for a recent review of those studies). Our feedback scheme is independent of time and geometry of the system; but it is likely that the efficiency of metal removal from the star forming regions varies with time, in dependence of the mass and size of the star-forming regions (see, e.g., Tenorio-Tagle et al. 2007; Wunsch et al. 2011). The development of winds and the fate of metals also depend on the geometry of the system: models with the same baryonic mass and SFH retain more or less metals, depending on their degree of flattening (see Recchi & Hensler 2013). Our code does not tackle the complex physics behind the circulation/loss of metals within/from the galaxy. On the other hand, thanks to its simplifications, it runs extremely fast, which makes it feasible to compute many hundreds of models and fully explore the parameter space.

Similarly to us, Calura & Menci (2009) also performed a post-processing of cosmological simulations for detailed chemistry and proposed that the realization probability of SNeIa in Local Group dwarf galaxies must be lower than in spirals such as the Milky Way. This assumption, joint to the adoption of strongly metal-enhanced outflows, allows them to reproduce the mass-metallicity relation of local dwarfs. However, they run models for generic dwarfs, while we are focusing here on a particular object, the Sculptor dSph. When we run models with lower values of the \mathcal{B} parameter (see Sect. 3.3) for Sculptor, we end up with theoretical MDFs narrower than observed. Furthermore, with this assumption we can not reproduce the steep knee in the $[\text{Mg}/\text{Fe}]$ versus $[\text{Fe}/\text{H}]$ relation that characterizes Sculptor’s stars. However, though we do not favour a low value for \mathcal{B} during the full evolution of Sculptor, we can not exclude a lower probability for SNIa events during the relatively early phases of Sculptor formation (see discussion in Sect. 4.3.1 and this section, forth paragraph).

We have already noticed a potential problem related to post-processing, namely, the differences in the cold gas masses computed with or without IRA (see Sect. 3.3.2). However, we have checked these are small (within a few per cent) in our models. Another issue is that of the lack of feedback from SNeIa in the adopted SAM. SNeIa keep exploding even if the star formation goes to zero. Therefore, while their effect is negligible when the star formation is active (because of the prevailing SNeII), one might expect they can play a role in keeping hot the ISM during halts in star formation activity. The final effect could be that of suppressing some of the late episodes of star formation in the models. Another potential problem of using a post-processing procedure is that the cooling curves used are metallicity dependent (Sutherland & Dopita 1993) and as the metallicities obtained in the post-processing are not necessarily identical to the SAM, this might lead to inconsistencies. However, we note that in the cases described here the metallicity distribution function obtained by the SAM and the post-processing chemical code are quite similar, therefore we do not expect the cooling processes to change very significantly. In the context of this work, we can only discuss such issues in a qualitative way. For a more robust, quantitative discussion, one should implement the chemical evolution equations in the SAM and compare the outputs of the self-consistent model with the results obtained with the post-processing

technique. This is however beyond the scope of this paper. Moreover, we like to note that implementing the full set of the chemical evolution equations in the SAM has its own problems: the computational time strongly increases because we must follow the evolution of each chemical species in each of the progenitors along the merger tree.

6 SUMMARY AND CONCLUSIONS

In this paper, we present a new chemical evolution model suited to follow the chemical evolution of dwarf galaxies in a full cosmological approach. The code adopts the histories of mass assembly and star formation derived from first principles by means of a hierarchical SAM and accounts for the contribution to the chemical enrichment from several stellar sources, namely, low- and intermediate-mass stars, massive stars and SNeIa. The lifetimes of stars of different initial masses are taken into account in detail, as is the distribution of the delay times for SNIa explosions. We adopt metallicity-dependent stellar yields that satisfactorily reproduce the trends of several abundance ratios with metallicity in the Milky Way. All of this is mandatory to study the abundance ratios of elements that have different stellar progenitors, which are precious diagnostics of the time-scales of structure formation and evolution.

In this study, we focus on the Sculptor dSph, for which high-quality data exist for a large number of stars, as a test bed for our model. We adopted mass assembly, star formation histories and gas flows for four different Sculptor-like models from the catalogue of satellite galaxies generated by the implementation of a version of the Munich SAM on the high-resolution Aquarius cosmological simulations (Starkenburg et al. 2013a) as a backbone for the post-processing chemical evolution code.

We find that, once a specific path is chosen for the formation of a dwarf galaxy inside a merging hierarchy of dark matter haloes, the shape of the MDF, as well as the behaviour of the abundance ratios as functions of $[\text{Fe}/\text{H}]$ in the system, are dictated primarily by the occurrence and strength of those physical processes able to remove[¶] a large fraction of the metals synthesized by the stars from the regions where the star formation occurs. From our results we conclude that in particular the tracks of $[\text{Mg}/\text{Fe}]$ and $[\text{Mn}/\text{Fe}]$ versus $[\text{Fe}/\text{H}]$ are powerful tracers of the mass assembly and star formation history of a galaxy.

All of our model galaxies have some problems in reproducing the whole body of abundance data available for the Sculptor dSph. This is true for our classical model, as well as for the ‘cosmological’ ones. For instance, none of the models matches the observed fraction of stars with $-2.5 < [\text{Fe}/\text{H}] < -2$. The cosmologically-motivated models also miss most of the stars that are found below $[\text{Fe}/\text{H}] < -2.5$. The problem we face is an ‘inverse’ G-dwarf problem, in the sense that we are severely underestimating the number of low-metallicity stars in the system. Possible solutions could involve higher efficiencies of metal losses during the early phases of galaxy formation, a diminished metal production from very metal-poor stars, or the presence of more gas to dilute the metals at early stages, without a corresponding increase in the star formation rate. In the metallicity range $-3 < [\text{Fe}/\text{H}] < -0.8$, all the models fit the available abundance data reasonably well.

[¶] Gas removal can result from internal (SN feedback, leading to a blow-out phase) or external (ram pressure stripping and/or tidal interactions by the Milky Way) mechanisms, or both, in our models.

As the infall of gas is fixed in the cosmologically motivated models, we can use our results to constrain the loss of metals needed and the mode of these metal losses. We find that the models prefer a significant dilution, in which supernova gas first interacts with the surrounding gas before it is lost forever from the star-forming medium of the galaxy.

ACKNOWLEDGEMENTS

The authors are indebted to Francesca Matteucci for having provided an earlier version of the classical chemical evolution code and to Vanessa Hill for having provided her data in advance of publication. The authors are indebted to the Aquarius Simulations Consortium; in particular, they are grateful to Gabriella De Lucia, Amina Helmi and Yang-Shyang Li for their role in developing the semi-analytic model of galaxy formation used in this paper. Several colleagues read an earlier version of this paper and provided insightful comments; they are: Francesco Calura, Thomas de Boer, Gabriella De Lucia, Amina Helmi, Vanessa Hill, Francesca Matteucci, Alan McConnachie, Monica Tosi and Kim Venn. The paper also greatly benefited from comments by an anonymous referee. DR and ES thank the International Space Science Institute (ISSI, Bern, CH) for support of the teams “Defining the full life-cycle of dwarf galaxy evolution: the Local Universe as a template” and “The Evolution of the First Stars in Dwarf Galaxies”. DR acknowledges partial financial support from PRIN INAF 2009, project “Formation and Early Evolution of Massive Star Clusters”, and PRIN MIUR 2010–2011, project “The Chemical and Dynamical Evolution of the Milky Way and Local Group Galaxies”, prot. 2010LY5N2T. ES is supported by the Canadian Institute for Advanced Research (CIFAR) Junior Academy and by a Canadian Institute for Theoretical Astrophysics (CITA) National Fellowship.

REFERENCES

- Arrigoni M., Trager S. C., Somerville R. S., Gibson B. K., 2010, *MNRAS*, 402, 173
- Battaglia G., Helmi A., Tolstoy E., Irwin M., Hill V., Jablonka P., 2008a, *ApJ*, 681, L13
- Battaglia G., Irwin M., Tolstoy E., Hill V., Helmi A., Letarte B., Jablonka P., 2008b, *MNRAS*, 383, 183
- Battaglia G., Helmi A., Morrison H., Harding P., Olszewski E. W., Mateo M., Freeman K. C., Norris J., Shectman S. A., 2005, *MNRAS*, 364, 433
- Bennett C. L., et al., 2012, preprint (arXiv:1212.5225)
- Bradamante F., Matteucci F., D’Ercole A., 1998, *A&A*, 337, 338
- Brook C. B., et al., 2012, *MNRAS*, 426, 690
- Calura F., Menci N., 2009, *MNRAS*, 400, 1347
- Cannon J. M., McClure-Griffiths N. M., Skillman E. D., Côté S., 2004, *ApJ*, 608, 768
- Carigi L., Hernandez X., 2008, *MNRAS*, 390, 582
- Carigi L., Colín P., Peimbert M., Sarmiento A., 1995, *ApJ*, 445, 98
- Carigi L., Hernandez X., Gilmore G., 2002, *MNRAS*, 334, 117
- Cescutti G., 2008, *A&A*, 481, 691
- Cescutti G., Matteucci F., Lanfranchi G. A., McWilliam A., 2008, *A&A*, 491, 401
- Chabrier G., 2003, *PASP*, 115, 763
- Chiosi C., Matteucci F., 1982, *A&A*, 110, 54
- Croton D. J., et al., 2006, *MNRAS*, 365, 11
- Da Costa G. S., 1984, *ApJ*, 285, 483
- de Boer T. J. L., 2012, PhD thesis, Kapteyn Astronomical Institute, Univ. Groningen
- de Boer T. J. L., et al., 2011, *A&A*, 528, A119

- de Boer T. J. L., Tolstoy E., Hill V., Saha A., Olsen K., Starkenburg E., Lemasle B., Irwin M. J., Battaglia G., 2012, *A&A*, 539, A103
- Dekel A., Silk J., 1986, *ApJ*, 303, 39
- De Lucia G., Blaizot J., 2007, *MNRAS*, 375, 2
- De Lucia G., Helmi A., 2008, *MNRAS*, 391, 14
- De Lucia G., Kauffmann G., White S. D. M., 2004, *MNRAS*, 349, 1101
- D’Ercole A., Brighenti F., 1999, *MNRAS*, 309, 941
- Dolphin A. E., 2002, *MNRAS*, 332, 91
- Ferrara A., Tolstoy E., 2000, *MNRAS*, 313, 291
- Font A. S., McCarthy I. G., Crain R. A., Theuns T., Schaye J., Wiersma R. P. C., Dalla Vecchia C., 2011, *MNRAS*, 416, 2802
- Frebel A., Kirby E. N., Simon J. D., 2010, *Nature*, 464, 72
- Fujita A., Mac Low M.-M., Ferrara A., Meiksin A., 2004, *ApJ*, 613, 159
- Geisler D., Smith V. V., Wallerstein G., Gonzalez G., Charbonnel C., 2005, *AJ*, 129, 1428
- Goswami A., Prantzos N., 2000, *A&A*, 359, 191
- Grevecich J., Putman M. E., 2009, *ApJ*, 696, 385
- Greggio L., 2005, *A&A*, 441, 1055
- Greggio L., Renzini A., 1983, *A&A*, 118, 217
- Grevesse N., Sauval A. J., 1998, *Space Sci. Rev.*, 85, 161
- Grieco V., Matteucci F., Pipino A., Cescutti G., 2012, *A&A*, 548, A60
- Guo Q., White S., Li C., Boylan-Kolchin M., 2010, *MNRAS*, 404, 1111
- Guo Q., White S., Angulo R. E., Henriques B., Lemson G., Boylan-Kolchin M., Thomas P., Short C., 2013, *MNRAS*, 428, 1351
- Heckman T. M., Sembach K. R., Meurer G. R., Strickland D. K., Martin C. L., Calzetti D., Leitherer C., 2001, *ApJ*, 554, 1021
- Helmi A., et al., 2006, *ApJ*, 651, L121
- Hunter D. A., Elmegreen B. G., 2004, *AJ*, 128, 2170
- Irwin M., Hatzidimitriou D., 1995, *MNRAS*, 277, 1354
- Iwamoto K., Brachwitz F., Nomoto K., Kishimoto N., Umeda H., Hix W. R., Thielemann F.-K., 1999, *ApJS*, 125, 439
- James B. L., Tsamis Y. G., Barlow M. J., 2010, *MNRAS*, 401, 759
- Kauffmann G., Colberg J. M., Diaferio A., White S. D. M., 1999, *MNRAS*, 307, 529
- Kennicutt R. C., Jr., 1989, *ApJ*, 344, 685
- Kirby E. N., Guhathakurta P., Sneden C., 2008, *ApJ*, 682, 1217
- Kirby E. N., Martin C. L., Finlator K., 2011b, *ApJ*, 742, L25
- Kirby E. N., Guhathakurta P., Bolte M., Sneden C., Geha M. C., 2009, *ApJ*, 705, 328
- Kirby E. N., Lanfranchi G. A., Simon J. D., Cohen J. G., Guhathakurta P., 2011a, *ApJ*, 727, 78
- Kirby E. N., et al., 2010, *ApJS*, 191, 352
- Kobayashi C., Nomoto K., 2009, *ApJ*, 707, 1466
- Kobayashi C., Tsujimoto T., Nomoto K., Hachisu I., Kato M., 1998, *ApJ*, 503, L155
- Kobulnicky H. A., Skillman E. D., 2008, *AJ*, 135, 527
- Komatsu E., et al., 2011 *ApJS*, 192, 18
- Kroupa P., 2001, *MNRAS*, 322, 231
- Kroupa P., 2012, in Stamatellos D., Goodwin S., Ward-Thompson D., eds, *The Labyrinth of Star Formation*, Springer, in press (arXiv:1210.1211)
- Lanfranchi G. A., Matteucci F., 2003, *MNRAS*, 345, 71
- Lanfranchi G. A., Matteucci F., 2004, *MNRAS*, 351, 1338
- Larson R. B., 1974, *MNRAS*, 169, 229
- Larson R. B., 1976, *MNRAS*, 176, 31
- Lemasle B., Hill V., Tolstoy E., Venn K. A., Shetrone M. D., Irwin M. J., de Boer T. J. L., Starkenburg E., Salvadori S., 2012, *A&A*, 538, A100
- Li W., Chornock R., Leaman J., Filippenko A. V., Poznanski D., Wang X., Ganeshalingam M., Mannucci F., 2011, *MNRAS*, 412, 1473
- Li Y.-S., White S. D. M., 2008, *MNRAS*, 384, 1459
- Li Y.-S., De Lucia G., Helmi A., 2010, *MNRAS*, 401, 2036
- Li Y.-S., Helmi A., De Lucia G., Stoehr F., 2009, *MNRAS*, 397, L87
- Mac Low M.-M., Ferrara A., 1999, *ApJ*, 513, 142
- Maeder A., 1992, *A&A*, 264, 105
- Marcolini A., D’Ercole A., Brighenti F., Recchi S., 2006, *MNRAS*, 371, 643
- Marconi G., Matteucci F., Tosi M., 1994, *MNRAS*, 270, 35
- Martin C. L., 1999, *ApJ*, 513, 156
- Martin C. L., Kobulnicky H. A., Heckman T. M., 2002, *ApJ*, 574, 663
- Mateo M. L., 1998, *ARA&A*, 36, 435
- Matteucci F., 2001, *The Chemical Evolution of the Galaxy*. Kluwer, Dordrecht
- Matteucci F., Chiosi C., 1983, *A&A*, 123, 121
- Matteucci F., Greggio L., 1986, *A&A*, 154, 279
- Matteucci F., Recchi S., 2001, *ApJ*, 558, 351
- Matteucci F., Tosi M., 1985, *MNRAS*, 217, 391
- Matteucci F., Panagia N., Pipino A., Mannucci F., Recchi S., Della Valle M., 2006, *MNRAS*, 372, 265
- Matteucci F., Spitoni E., Recchi S., Valiante R., 2009, *A&A*, 501, 531
- Meurer G. R., Freeman K. C., Dopita M. A., Cacciari C., 1992, *AJ*, 103, 60
- Mo H. J., Mao S., White S. D. M., 1998, *MNRAS*, 295, 319
- Moster B. P., Somerville R. S., Maulbetsch C., van den Bosch F. C., Macciò A. V., Naab T., Oser L., 2010, *ApJ*, 710, 903
- Mouhcine M., Contini T., 2002, *A&A*, 389, 106
- Nagashima M., Okamoto T., 2006, *ApJ*, 643, 863
- Nagashima M., Lacey C. G., Okamoto T., Baugh C. M., Frenk C. S., Cole S., 2005, *MNRAS*, 363, L31
- North P., et al., 2012, *A&A*, 541, A45
- Okamoto T., Frenk C. S., Jenkins A., Theuns T., 2010, *MNRAS*, 406, 208
- Oppenheimer B. D., Davé R., 2006, *MNRAS*, 373, 1265
- Peeples M. S., Shankar F., 2011, *MNRAS*, 417, 2962
- Pietrzyński G., Gieren W., Szewczyk O., Walker A., Rizzi L., Bresolin F., Kudritzki R.-P., Nalewajko K., Storm J., Dall’Ora M., Ivanov V., 2008, *AJ*, 135, 1993
- Pilkington K., et al., 2012, *MNRAS*, 425, 969
- Pilyugin L. S., 1993, *A&A*, 277, 42
- Pipino A., Devriendt J. E. G., Thomas D., Silk J., Kaviraj S., 2009, *A&A*, 505, 1075
- Pustilnik S. A., Kniazev A. Y., Pramskij A. G., Ugryumov A. V., Masegosa J., 2003, *A&A*, 409, 917
- Putman M. E., Bureau M., Mould J. R., Staveley-Smith L., Freeman K. C., 1998, *AJ*, 115, 2345
- Rahimi A., Kawata D., Allende Prieto C., Brook C. B., Gibson B. K., Kiessling A., 2011, *MNRAS*, 415, 1469
- Recchi S., Hensler G., 2013, *A&A*, 551, A41
- Recchi S., Matteucci F., D’Ercole A., 2001, *MNRAS*, 322, 800
- Revaz Y., Jablonka P., 2012, *A&A*, 538, 82
- Romano D., Cescutti G., Matteucci F., 2011, *MNRAS*, 418, 696
- Romano D., Tosi M., Matteucci F., 2006, *MNRAS*, 365, 759
- Romano D., Karakas A. I., Tosi M., Matteucci F., 2010a, *A&A*, 522, A32
- Romano D., Tosi M., Cignoni M., Matteucci F., Pancino E., Bellazzini M., 2010b, *MNRAS*, 401, 2490
- Saito M., 1979, *PASJ*, 31, 193
- Sakamoto T., Chiba M., Beers T. C., 2003, *A&A*, 397, 899
- Salpeter E. E., 1955, *ApJ*, 121, 161
- Salvadori S., Ferrara A., Schneider R., 2008, *MNRAS*, 386, 348
- Sawala T., Scannapieco C., Maio U., White S., 2010, *MNRAS*, 402, 1599
- Schaller G., Schaerer D., Meynet G., Maeder A., 1992, *A&AS*, 96, 269
- Schmidt M., 1963, *ApJ*, 137, 758
- Searle L., Zinn R., 1978, *ApJ*, 225, 357
- Shapley H., 1938, *Harvard College Obs. Bulletin*, 908, 1
- Shetrone M. D., Côté P., Sargent W. L. W., 2001, *ApJ*, 548, 592
- Shetrone M., Venn K. A., Tolstoy E., Primas F., Hill V., Kaufer A., 2003, *AJ*, 125, 684
- Silich S. A., Tenorio-Tagle G., 1998, *MNRAS*, 299, 249
- Smith M. C., et al., 2007, *MNRAS*, 379, 755
- Spite M., et al., 2005, *A&A*, 430, 655
- Springel V., et al., 2005, *Nature*, 435, 629
- Springel V., Wang J., Vogelsberger M., Ludlow A., Jenkins A., Helmi A., Navarro J. F., Frenk C. S., White S. D. M., 2008a, *MNRAS*, 391, 1685
- Springel V., White S. D. M., Frenk C. S., Navarro J. F., Jenkins A., Vogelsberger M., Wang J., Ludlow A., Helmi A., 2008b, *Nature*, 456, 73
- Springel V., White S. D. M., Tormen G., Kauffmann G., 2001, *MNRAS*, 328, 726
- Starkenburg E., et al., 2010, *A&A*, 513, A34
- Starkenburg E., et al., 2013a, *MNRAS*, 429, 725
- Starkenburg E., et al., 2013b, *A&A*, 549, A88
- Stil J. M., Israel F. P., 2002, *A&A*, 392, 473

- Summers L. K., Stevens I. R., Strickland D. K., 2001, *MNRAS*, 327, 385
 Summers L. K., Stevens I. R., Strickland D. K., Heckman T. M., 2003, *MNRAS*, 342, 690
 Sutherland R. S., Dopita M. A., 1993, *ApJS*, 88, 253
 Tafelmeyer M., et al., 2010, *A&A*, 524, A58
 Talbot R. J. Jr., Arnett W. D., 1973, *ApJ*, 186, 51
 Tenorio-Tagle G., Wünsch R., Silich S., Palouš J., 2007, *ApJ*, 658, 1196
 Thomas D., 1999, *MNRAS*, 306, 655
 Timmes F. X., Woosley S. E., Weaver T. A., 1995, *ApJS*, 98, 617
 Tinsley B. M., 1980, *Fundam. Cosm. Phys.*, 5, 287
 Tolstoy E., Venn K. A., Shetrone M., Primas F., Hill V., Kaufer A., Szeifert T., 2003, *AJ*, 125, 707
 Tolstoy E., et al., 2004, *ApJ*, 617, L119
 Tolstoy E., et al., 2006, *Messenger*, 123, 33
 Tolstoy E., Hill V., Tosi M., 2009, *ARA&A*, 47, 371
 Vader J. P., 1987, *ApJ*, 317, 128
 van den Hoek L. B., Groenewegen M. A. T., 1997, *A&AS*, 123, 305
 Veilleux S., Cecil G., Bland-Hawthorn J., 2005, *ARA&A*, 43, 769
 Venn K. A., et al., 2012, *ApJ*, 751, 102
 Wang J., De Lucia G., Kitzbichler M. G., White S. D. M., 2008, *MNRAS*, 384, 1301
 Westfall K. B., Majewski S. R., Ostheimer J. C., Frinchaboy P. M., Kunkel W. E., Patterson R. J., Link R., 2006, *AJ*, 131, 375
 White S. D. M., Frenk C. S., 1991, *ApJ*, 379, 52
 White S. D. M., Rees M. J., 1978, *MNRAS*, 183, 341
 Wiersma R. P. C., Schaye J., Smith B. D., 2009, *MNRAS*, 393, 99
 Wilkinson M. I., Evans N. W., 1999, *MNRAS*, 310, 645
 Woosley S. E., Weaver T. A., 1995, *ApJS*, 101, 181
 Wünsch R., Silich S., Palouš J., Tenorio-Tagle G., Muñoz-Tuñón C., 2011, *ApJ*, 740, 75
 Xue X. X., et al., 2008, *ApJ*, 684, 1143
 Yin J., Matteucci F., Vladilo G., 2011, *A&A*, 531, 136

APPENDIX A: THE SCULPTOR MDF

Both the DART project (Tolstoy et al. 2006; Helmi et al. 2006; Battaglia et al. 2008b; Starkenburg et al. 2010) and Kirby et al. (2009, 2010) provide spectroscopic datasets of large samples of individual RGB stars within the Sculptor dwarf galaxy. However, since each dataset has its own observational biases with respect to its radial extent and depth, the resulting MDFs are quite different. In this Appendix, we strive to combine the two datasets available in order to remove the observational biases as much as possible and obtain a MDF that is representing all stellar populations of the Sculptor dwarf galaxy.

Firstly, the sample from the DART project provides metallicities derived through measurements of the Ca II triplet line strengths for over 600 stars in Sculptor out to $\sim 1.5^\circ$ in elliptical radii (Tolstoy et al. 2006; Helmi et al. 2006; Battaglia et al. 2008b). The MDF for the sample is derived using the latest calibration of Ca II triplet line strengths to $[\text{Fe}/\text{H}]$ (Starkenburg et al. 2010). Additionally, a high-resolution multi-object study was carried out in the centre of the galaxy by DART (Hill et al., in preparation). The $[\text{Fe}/\text{H}]$ values derived from individual Fe lines in this high-resolution study do agree well with the measurements of $[\text{Fe}/\text{H}]$ via the strong Ca II triplet lines for the stars overlapping in both the low- and high-resolution samples (Battaglia et al. 2008b; Starkenburg et al. 2010). Although the DART dataset goes down to faint magnitudes ($V \sim 20$) in the outskirts of the galaxy, the central sample only fully covers the brightest ~ 1 magnitude below the tip of the RGB (until $V \sim 18$). As shown by de Boer et al. (2012), this results in a bias in the MDF in this region of the galaxy, as low-metallicity stellar populations are underrepresented on the upper RGB. They

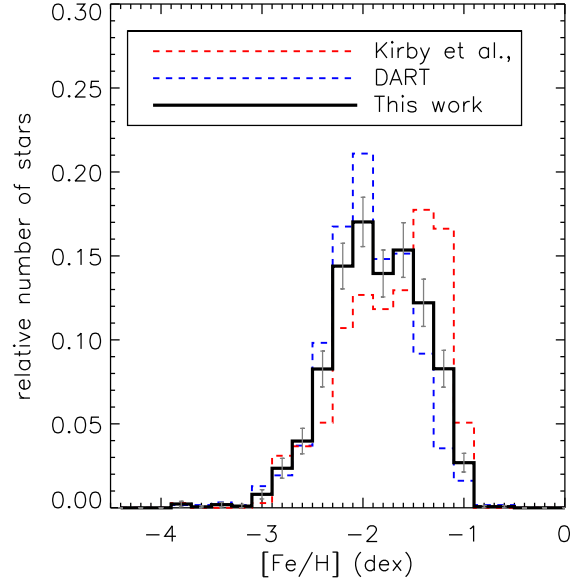


Figure A1. The MDFs from Kirby et al. (2009; red dashed line) and the DART collaboration (see Tolstoy et al. 2006; Helmi et al. 2006; Battaglia et al. 2008b; Starkenburg et al. 2010; blue dashed line), from which the MDF as used in this work has been derived (see text for details). The final MDF is shown as the thick black line. Poissonian errorbars are also shown.

conclude that a coverage down to $V = 19.5$ is at least required to obtain an unbiased MDF.

Secondly, Kirby et al. (2009, 2010) present a MDF from spectroscopic observations of nearly 400 RGB stars distributed within $\sim 0.2^\circ$ in elliptical radii. The resolution of their study is comparable to the low-resolution DART study, but their spectra cover a larger wavelength region. To derive $[\text{Fe}/\text{H}]$ and abundance ratios for several α elements they apply a spectral synthesis technique (see Kirby et al. 2008 for details). They find very good agreement when comparing results for stars overlapping with the high-resolution sample of Hill et al. (in preparation), presented in Battaglia et al. (2008b). Their MDF is also shown to be comparable to the DART MDF if the same radial and magnitude cuts are applied to both samples (see de Boer et al. 2012, their figure 6, where they show that for $r_{\text{ell}} \leq 0.2^\circ$ and truncation at $V \simeq 18$ the two MDFs are the same within the respective errorbars). The stars studied in Kirby et al. (2009, 2010) go down to sufficiently faint magnitudes to expect an unbiased sample in depth. However, an observational bias is expected because of the limited radial extent of their survey. The Sculptor dwarf galaxy is known to have a strong metallicity gradient with radius (Tolstoy et al. 2004; Westfall et al. 2006), as well as an age gradient (de Boer et al. 2012). The sample from Kirby et al. (2009) covers only the inner parts of the galaxy and, therefore, undersamples the older and more metal-poor stellar population.

In Fig. A1 the MDFs from DART and Kirby et al. (2009) are both shown, as blue and red dashed lines, respectively. Both MDFs shown here are truncated at $V = 20$ to ensure that both datasets used are equally deep. Additionally, this magnitude cut-off gets rid of the worst S/N data. Clearly, the shapes and peaks of the two MDFs do not agree. The apparent bimodality in the observed MDF from Kirby et al. (2009) present as two peaks at $[\text{Fe}/\text{H}] = -2.1$ and -1.3 dex (of which the more metal-rich is the dominant) is not seen in the larger and more radially extended DART sample,

Table A1. Tabulated MDF for the final sample of about 1000 stars presented in this work. This is shown as the thick black line in Fig. A1.

[Fe/H] (dex) (1)	Rel. # (2)	Error (3)	[Fe/H] (dex) (4)	Rel. # (5)	Error (6)
−4.4	0.00	0.00	−1.8	1.39e-01	1.40e-02
−4.2	0.00	0.00	−1.6	1.53e-01	1.63e-02
−4.0	0.00	0.00	−1.4	1.22e-01	1.41e-02
−3.8	2.27e-03	1.61e-03	−1.2	8.28e-02	1.10e-02
−3.6	5.77e-04	5.77e-04	−1.0	2.69e-02	5.55e-03
−3.4	1.88e-03	1.34e-03	−0.8	6.73e-04	6.73e-04
−3.2	1.01e-03	1.01e-03	−0.6	6.73e-04	6.73e-04
−3.0	8.02e-03	2.76e-03	−0.4	0.00	0.00
−2.8	2.35e-02	5.91e-03	−0.2	0.00	0.00
−2.6	3.97e-02	7.57e-03	0.0	0.00	0.00
−2.4	8.26e-02	1.07e-02	0.2	0.00	0.00
−2.2	1.44e-01	1.36e-02	0.4	0.00	0.00
−2.0	1.70e-01	1.47e-02			

Note. Different columns list: (1) and (4) the central value of the metallicity bin; (2) and (5) the relative number of stars within the metallicity bin; (3) and (6) the Poissonian error in the relative number of stars.

which peaks at lower metallicity. To create a more homogeneous sample, we recalculate the elliptical radius for each star in either sample using the best-fit parameters from the photometric study of de Boer et al. (2011). Subsequently we bin both samples in bins of 0.05° in elliptical radius and construct a separate MDF for each bin. We decided to use solely the sample of Kirby et al. (2009) as a representant sample for the inner regions of the galaxy ($r_{\text{ell}} < 0.2^\circ$) due to its greater observational depth and thus completeness, while we use the DART sample to represent the outer regions ($0.2^\circ < r_{\text{ell}} < 1.5^\circ$). Following Battaglia et al. (2008a) we represent the surface density of RGB stars in the Sculptor dSph by a combined Plummer and Sersic profile with half-light radii of 15.1 and 8.6 arcmins, respectively. By multiplying the surface density and the area of each bin in elliptical radius, we obtain the weight each bin contributes to the galaxy. Normalizing these weights we find that the relative contribution from the inner bins ($r_{\text{ell}} < 0.2^\circ$) is roughly half of the total (48 per cent). The final relative MDF, shown in Fig. A1 (entries are listed in Table A1), consists of all MDFs of each radius bin multiplied with their relative weight. Throughout this work we will use this final MDF as a representative MDF for the full Sculptor galaxy and as such compare it directly to our models.

This paper has been produced using the Royal Astronomical Society/Blackwell Science L^AT_EX style file.